

# Collective P-Wave Orbital Dynamics of Ultracold Fermions

Mikhail Mamaev,<sup>1,2,\*</sup> Peiru He,<sup>1,2</sup> Thomas Bilitewski,<sup>1,2</sup> Vijin Venu,<sup>3</sup> Joseph H. Thywissen,<sup>3</sup> and Ana Maria Rey<sup>1,2</sup>

<sup>1</sup>*JILA, NIST, and Department of Physics, University of Colorado, Boulder, CO 80309, USA*

<sup>2</sup>*Center for Theory of Quantum Matter, University of Colorado, Boulder, CO 80309, USA*

<sup>3</sup>*Department of Physics and CQIQC, University of Toronto, Ontario M5S 1A7, Canada*

(Dated: June 22, 2022)

We introduce a protocol to observe p-wave interactions in ultracold fermionic atoms loaded in a three-dimensional optical lattice. Our scheme uses specific motionally excited band states to form an orbital subspace immune to band relaxation. A laser dressing is applied to reduce the differential kinetic energy of the orbital states and make their dispersion highly isotropic. When combined with a moderate increase of the scattering volume by a Feshbach resonance, the effect of p-wave interactions between the orbitals can be observed from the system dynamics on realistic timescales. By considering the evolution of ferromagnetic product states, we further explore parameter regimes where collective enhancement of p-wave physics facilitated by a many-body gap enables us to map the complex extended Fermi-Hubbard Hamiltonian of the system to a simple one-axis twisting model. Experimental protocols to probe the resulting many-body dynamics, state preparation, and detection are presented, including the effects of particle loss, spin-orbit coupling, and doping.

**Introduction.** Ultracold quantum gases in optical lattices are among the leading platforms for quantum simulation of strongly correlated matter, non-equilibrium dynamics, and lattice superfluidity. While there has been impressive experimental progress [1, 2], most investigations thus far have been limited to s-wave interacting systems in the lowest motional band. A fascinating avenue yet to be explored experimentally is many-body lattice physics with p-wave interactions [3, 4] in higher bands. P-wave interacting systems can host long-sought phases including topological superfluids, Majorana fermions [5–7], and itinerant ferromagnetism [8, 9]. At the same time, atoms in higher bands are a unique resource [10] for emulating orbital degrees of freedom in real materials [11] which give rise to heavy fermions [12], RKKY interactions [13], and orbitally ordered Mott phases [14, 15].

Despite these attractive features, control and manipulation of p-wave interacting gases has remained a challenge for ultracold atom experiments. The timescales on which p-wave interactions contribute to dynamics tend to be slow compared to coherence times [16] and lossy when increased by a Feshbach resonance [17–19]. Moreover, collisions in higher bands suffer from band relaxation [20, 21]. Progress in mitigating relaxation via designed lattice geometries has lead to improvements [22–24], but further advances are required to explore the full range of orbital physics in optical lattices.

In this work, we present protocols to engineer a generalized p-wave Fermi-Hubbard model and probe the interaction-induced dynamics of ultracold polarized fermionic atoms loaded in excited orbitals of optical lattices. Our protocol is robust to both p-wave losses and band relaxation. The excited bands provide the necessary degree of freedom for the construction of orbitally antisymmetric two-atom wavefunctions that interact on-site with p-wave interactions using spin-polarized atoms. Orbital dynamics in first excited bands are stabilized via Pauli blocking by preparing a completely filled ground band, thus mimicking the conventional conduction-band configuration of materials. We consider a quasi-two-dimensional (2D) geometry in which Bragg dressing modifies the dispersion relation by suppressing its orbital anisotropy. This dramatically simplifies the many-body dynamics, allow-

ing an accurate mapping of the p-wave Fermi-Hubbard model to an XXZ model, with the conventional magnetic spin states replaced by orbital states. We delineate a specific regime in which the dynamics can be further mapped to a collective one-axis twisting (OAT) model thanks to the opening of a many-body gap [25]. We discuss the required state preparation and how the many-body p-wave dynamics can be observed with a Ramsey protocol. Our proposal offers new ways to understand p-wave orbital physics in an experimentally accessible regime where elastic interactions dominate over inelastic collisions and other decoherence processes.

**P-wave Fermi-Hubbard model.** The system we consider is a three-dimensional (3D) optical lattice loaded with spin-polarized fermionic alkali atoms in their ground electronic state. The lattice depths are  $(V_X, V_Y, V_Z)E_r$  with  $E_r$  the recoil energy, and we assume that  $V_X = V_Y \ll V_Z$ , confining the system to a stack of independent 2D planes each with  $L = L_X L_Y$  sites populated by  $N$  atoms. We work in the ultracold regime where atoms are first cooled into the lowest motional band, and then some of them are transferred to specific excited band states. The three relevant orbital levels can be written as

$$\begin{aligned} |g\rangle &= w_0^X(X)w_0^Y(Y)w_0^Z(Z), \\ |\uparrow\rangle &= w_1^X(X)w_0^Y(Y)w_0^Z(Z), \text{ and} \\ |\downarrow\rangle &= w_0^X(X)w_1^Y(Y)w_0^Z(Z), \end{aligned} \quad (1)$$

where  $w_n^\nu$  is the  $n$ -th lattice Wannier function along the  $\nu \in \{X, Y, Z\}$  direction. As shown in Fig. 1, our desired configuration is a filling of  $N/L=2$ : each site will have one atom in  $|g\rangle$ , creating a filled ground band, and a second atom in the subspace of  $\{|\uparrow\rangle, |\downarrow\rangle\}$  acting as a spin-1/2 degree of freedom. The occupation of the ground state prevents collisional relaxation since any energy-conserving two-atom process would need to move an atom down to the ground band; here, this is forbidden by Pauli exclusion.

The low-energy Hamiltonian can be written as an anisotropic extended Fermi-Hubbard model (Supplemental Material A [26]),

$$\hat{H}_{\text{FH}} = \hat{H}_J + \hat{H}_{\text{int}}^{(\text{OS})} + \hat{H}_{\text{int}}^{(\text{CS})}. \quad (2)$$

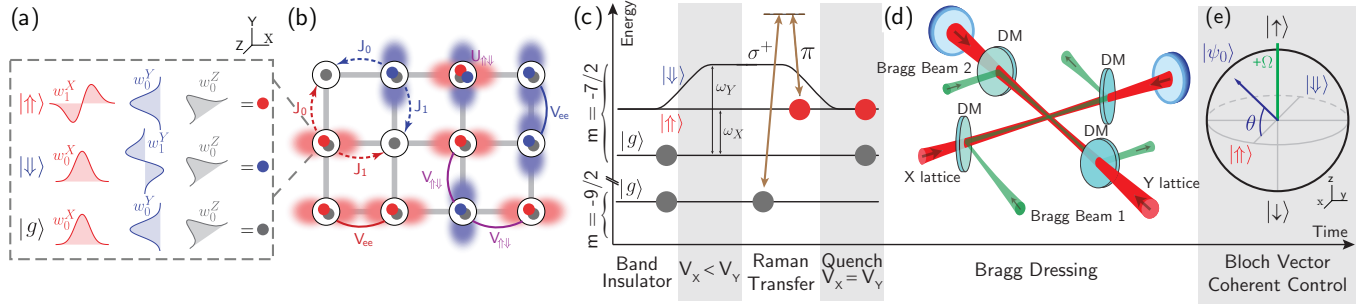


FIG. 1. Proposal elements. (a) Band scheme within a 3D optical lattice: the  $|g\rangle$  state describes ground band atoms with harmonic excitation numbers  $(0, 0, 0)$  along  $(X, Y, Z)$ ; the  $|\uparrow\rangle$  and  $|\downarrow\rangle$  states, with excitations  $(1, 0, 0)$  or  $(0, 1, 0)$  respectively, are singly-excited band states along the  $X$  or  $Y$  directions of the 2D plane. The  $|g\rangle$  band is filled by an atom on every site. The  $|\uparrow\rangle$  and  $|\downarrow\rangle$  are half-filled with one additional atom per site, forming an effective spin-1/2 subspace. (b) Fermi-Hubbard physics on a single  $X$ - $Y$  plane. The  $|\uparrow\rangle$  and  $|\downarrow\rangle$  atoms tunnel at rates  $J_0$  and  $J_1$  along their ground and excited directions respectively. There is an on-site p-wave interaction  $U_{\uparrow\downarrow}$  between  $|\uparrow\rangle$ ,  $|\downarrow\rangle$  atoms, as well as nearest-neighbour interactions  $V_{ee}$ ,  $V_{\uparrow\downarrow}$ . (c) State preparation. Using ultracold  $^{40}\text{K}$  atoms as an example, one starts with a band insulator of two ground band atoms per site in two nuclear-spin states  $|m = -9/2\rangle$ ,  $|m = -7/2\rangle$  of the ground hyperfine manifold. The lattice depths are set to  $V_X < V_Y$ , causing the  $|\uparrow\rangle$  state to be lower in energy than  $|\downarrow\rangle$ . The  $|-9/2, g\rangle$  ground-band atom is transferred to the  $|-7/2, \uparrow\rangle$  state using a Raman transition with one linearly- and one circularly-polarized beam through an intermediate state such as the electronic  $^2P_{1/2}$ ,  $|F = 7/2, m = -7/2\rangle$  state. The  $V_Y$  depth is then quenched to match  $V_X$ . (d) Bragg dressing can be implemented with beams (shown in green) that co-propagate with the lattice beams (red), when the Bragg-laser wavelength is half that of the lattice beams. The out-of-plane lattice beam is not shown. (e) The state  $|\uparrow\rangle$  is an equal superposition of the two flavors of the Bragg-dressed basis. Using standard coherent control protocols, any direction of the Bloch vector can be chosen.

Here  $\hat{H}_J$  describes the kinetic energy of the atoms, which tunnel to nearest neighbour sites at rate  $J_0$  or  $J_1$  depending on the tunneling direction and orbital: the  $|\uparrow\rangle$  atoms tunnel at rate  $J_1$  along  $X$  and rate  $J_0$  along  $Y$ , while the  $|\downarrow\rangle$  atoms do the opposite. In general  $J_1 \gg J_0$  since excited states have a larger spatial extent along their excitation direction [see Fig. 1(a)]. This anisotropy causes tunneling to take the form

$$\hat{H}_J = \sum_{\vec{k}} \epsilon_{\vec{k}} \left( \hat{n}_{\vec{k},\uparrow} - \hat{n}_{\vec{k},\downarrow} \right) + \sum_{\vec{k}} \bar{E}_{\vec{k}} \left( \hat{n}_{\vec{k},\uparrow} + \hat{n}_{\vec{k},\downarrow} \right), \quad (3)$$

with  $\epsilon_{\vec{k}} = (J_1 + J_0)(\cos k_X - \cos k_Y)$  and  $\bar{E}_{\vec{k}} = (J_1 - J_0)(\cos k_X + \cos k_Y)$ . Here  $\hat{n}_{\vec{k},\gamma} = \hat{c}_{\vec{k},\gamma}^\dagger \hat{c}_{\vec{k},\gamma}$  and  $\hat{c}_{\vec{k},\gamma} = L^{-1/2} \sum_{\vec{r}} e^{i\vec{r}\cdot\vec{k}} \hat{c}_{\vec{r},\gamma}$ , with  $\vec{k} = (k_X, k_Y)$  the lattice quasi-momentum and  $\hat{c}_{\vec{r},\gamma}$  annihilating an atom on lattice site  $\vec{r}$  in band state  $\gamma \in \{\uparrow, \downarrow\}$ .

The remainder of  $\hat{H}_{\text{FH}}$  contains the interactions, which are only p-wave since s-wave collisions are forbidden for a spin-polarized gas. The on-site contribution is

$$\hat{H}_{\text{int}}^{(\text{OS})} \approx U_{\uparrow\downarrow} \sum_{\vec{r}} \hat{n}_{\vec{r},\uparrow} \hat{n}_{\vec{r},\downarrow}, \quad (4)$$

where  $U_{\uparrow\downarrow}$  is the p-wave interaction coefficient between one  $|\uparrow\rangle$  atom and one  $|\downarrow\rangle$  atom in the same site. This interaction coefficient is proportional to p-wave overlap integrals defined by a p-wave pseudopotential, differing from conventional s-wave pseudopotential as it involves gradients of the Wannier orbitals (Supplementary Material A [26]). The interactions are also proportional to a scattering volume  $b_{XY}^3$  controlled by a Feshbach resonance. In principle there can be two different scattering volumes due to dipole-dipole splitting of the

closed channels, but we assume that the magnetic field is oriented along  $Z$ , causing only the transverse volume to be relevant. On-site terms describing interactions between  $|g\rangle$  and  $|\uparrow\rangle$ , and between  $|g\rangle$  and  $|\downarrow\rangle$ , are constants of motion and can be dropped.

For a sufficiently deep lattice potential  $V_X = V_Y \gg 1$ , aside from the on-site terms only the nearest-neighbour interactions are non-negligible. These are stronger than analogous cross-site s-wave interactions would be for the same lattice depth, since the associated spatial overlap integrals involve gradients of the Wannier functions. Just like p-band tunneling, the cross-site p-wave interactions are anisotropic and depend on the scattering volume  $b_{XY}^3$ , spatial orientations, and orbitals of the interacting particles [see Fig. 1(b)]. The dominant cross-site terms are

$$\begin{aligned} \hat{H}_{\text{int}}^{(\text{CS})} \approx & \sum_{\vec{r}, \gamma=\uparrow, \downarrow} [V_{ee} \hat{n}_{\vec{r},\gamma} \hat{n}_{\vec{r}+\vec{\nu}_{\gamma},\gamma} \\ & + V_{\uparrow\downarrow} (\hat{n}_{\vec{r},\uparrow} \hat{n}_{\vec{r}+\vec{\nu}_{\gamma},\downarrow} + \hat{n}_{\vec{r},\downarrow} \hat{n}_{\vec{r}+\vec{\nu}_{\gamma},\uparrow})]. \end{aligned} \quad (5)$$

Here  $\vec{\nu}_{\gamma}$  is a lattice unit vector along the  $X, Y$  direction for  $\gamma = \uparrow, \downarrow$  respectively. The interaction  $V_{ee}$  is between two atoms in the same orbital  $\gamma$ , one located at  $\vec{r}$  and another at  $\vec{r} + \vec{\nu}_{\gamma}$ .  $V_{\uparrow\downarrow}$  is the interaction between nearest neighbour atoms in different excited orbitals. For  $^{40}\text{K}$  and  $V_X = V_Y = 25$ ,  $V_Z = 100$ ,  $b_{XY} = 292a_0$  with  $a_0$  the Bohr radius (a 20-fold increase in background volume), one finds  $J_0 = 5\text{Hz}$ ,  $J_1 = 133\text{Hz}$ ,  $U_{\uparrow\downarrow} = 900\text{Hz}$ ,  $V_{ee} = 0.3\text{Hz}$ ,  $V_{\uparrow\downarrow} = 0.1\text{Hz}$  (Supplemental Material A [26]). These parameters are used in the following, unless otherwise specified.

*Momentum-space spin model.* The implementation of an anisotropic extended Fermi-Hubbard model, Eq. (2), offers exciting opportunities for quantum simulation [27]. However,

we are specifically interested in collective dynamics induced by p-wave interactions. To favor ordering of these orbital degrees of freedom one can reduce competitive depolarization from the kinetic terms  $\hat{H}_J$  with the introduction of a laser field that couples  $|\uparrow\uparrow\rangle$  and  $|\downarrow\downarrow\rangle$  (Supplemental Material B [26]):

$$\hat{H}_\Omega = \frac{\Omega}{2} \sum_{\vec{k}} \left( \hat{c}_{\vec{k},\uparrow}^\dagger \hat{c}_{\vec{k},\downarrow} + h.c. \right). \quad (6)$$

Experimentally, such a term is generated by an optical field whose Bragg grating is oriented along a diagonal reciprocal lattice vector [see Fig. 1(d)]. We assume that the drive couples only atoms with equal quasi-momentum, which can be ensured with appropriate laser wavelengths and orientation (Supplemental Material B [26]). Dressed with this coupling, the single-particle eigenenergies change from  $\overline{E}_{\vec{k}} \pm \epsilon_{\vec{k}}$  to  $\overline{E}_{\vec{k}} \pm \sqrt{\epsilon_{\vec{k}}^2 + (\Omega/2)^2}$ . When  $\Omega \gg |\epsilon_{\vec{k}}|$ , the anisotropic part of the spectrum  $\epsilon_{\vec{k}}$  is flattened, which allows interactions to play a more dominant role in the dynamics; the flattened spectrum suppresses quasi-momentum-changing collisions and keeps each atom frozen in a given mode when evolving from a collective initial product state. In this regime we can approximate the Fermi-Hubbard model with a spin-1/2 model  $\hat{H}_{\text{FH}} + \hat{H}_\Omega \approx \hat{H}_S$  (Supplemental Material C [26]):

$$\hat{H}_S = \sum_{\vec{k},\vec{k}'} U_{\vec{k},\vec{k}'} \vec{\sigma}_{\vec{k}} \cdot \vec{\sigma}_{\vec{k}'} + \sum_{\vec{k},\vec{k}'} V_{\vec{k},\vec{k}'} \hat{\sigma}_{\vec{k}}^x \hat{\sigma}_{\vec{k}'}^x + \sum_{\vec{k}} \left( \epsilon_{\vec{k}} \hat{\sigma}_{\vec{k}}^x + \frac{\Omega}{2} \hat{\sigma}_{\vec{k}}^z \right), \quad (7)$$

with coefficients

$$\begin{aligned} U_{\vec{k},\vec{k}'} &= -\frac{U_{\uparrow\downarrow}}{4L} - \frac{V_{\uparrow\downarrow}}{2L} [\cos(k_X - k'_X) + \cos(k_Y - k'_Y)], \\ V_{\vec{k},\vec{k}'} &= \frac{V_{ee} - 2V_{\uparrow\downarrow}}{4L} [2 - \cos(k_X - k'_X) - \cos(k_Y - k'_Y)]. \end{aligned} \quad (8)$$

Here we define spin operators  $\hat{\sigma}_{\vec{k}}^\alpha = \hat{a}_{\vec{k},\mu}^\dagger \sigma_{\mu\mu'}^\alpha \hat{a}_{\vec{k},\mu'}$ , with  $\sigma^\alpha$  the standard  $2 \times 2$  Pauli matrices for  $\alpha \in \{x, y, z\}$ , summing over new dressed atom flavors  $\mu, \mu' \in \{\uparrow, \downarrow\}$  defined as eigenstates of the drive:

$$\hat{a}_{\vec{k},\uparrow} = \frac{1}{\sqrt{2}} (\hat{c}_{\vec{k},\uparrow} + \hat{c}_{\vec{k},\downarrow}) \text{ and } \hat{a}_{\vec{k},\downarrow} = \frac{1}{\sqrt{2}} (\hat{c}_{\vec{k},\uparrow} - \hat{c}_{\vec{k},\downarrow}). \quad (9)$$

Note that the on-site contribution proportional to  $U_{\uparrow\downarrow}$  is SU(2) symmetric, because only the orbital singlet state of the two excited bands can interact. This spin model is valid in the regime where the collisional rate for relaxing the motional degrees of freedom is slower than the internal spin exchange dynamics.

*Ramsey spectroscopy protocol.* We initialize a collective product state  $|\psi_0\rangle = \prod_{\vec{k}} |\rightarrow\rangle_{\vec{k}} = \prod_{\vec{k}} |\uparrow\rangle_{\vec{k}}$ , i.e. with spins pointing along the  $x$  direction of the dressed Bloch sphere. The preparation of this state is depicted in Fig. 1(c). We start from a standard band insulator with double occupancy in the ground band, using the two lowest-energy hyperfine states of the ground electronic state (a small hole fraction can also be tolerated, see Supplemental Material E [26]). The lattice depths along  $X$  and  $Y$  are made unequal with  $V_Y > V_X$ , so that the  $|\downarrow\downarrow\rangle$  state is higher in energy than  $|\uparrow\uparrow\rangle$ . A spin-polarized two-band insulator is created with a sideband-resolved Raman

pulse. The  $V_Y$  lattice depth is then quenched to match  $V_X$ . This state can be written as a superposition of the drive eigenstates  $|\uparrow\downarrow\rangle_{\vec{k}} = |\rightarrow\rangle_{\vec{k}} = (|\uparrow\rangle_{\vec{k}} + |\downarrow\rangle_{\vec{k}})/\sqrt{2}$ , pointing along the  $x$ -axis of the collective Bloch sphere. We will also consider cases when another pulse is applied to incline the initial state by an angle  $\theta$  from the  $x$ -axis,

$$|\psi_0\rangle = e^{i\theta \hat{S}^y} \prod_{\vec{k}} |\rightarrow\rangle_{\vec{k}}, \quad (10)$$

where  $\hat{S}^{\alpha=x,y,z} = \frac{1}{2} \sum_{\vec{k}} \hat{\sigma}_{\vec{k}}^{\alpha=x,y,z}$  are collective-spin operators [see Fig. 1(e)]. The Ramsey protocol [Fig. 2(a)] measures the dynamics of the collective observables

$$\langle \hat{S}^- \rangle = \langle \hat{S}_x \rangle + i \langle \hat{S}_y \rangle \equiv C(t) e^{i\phi(t)} \quad (11)$$

after time  $t$ . Here  $C = (\langle \hat{S}^x \rangle^2 + \langle \hat{S}^y \rangle^2)^{1/2}$  is the contrast, and  $\phi = \arg \langle \hat{S}^- \rangle$  an interaction-induced phase shift. To remove the fast single particle rotation induced by the drive we flip the sign of  $\Omega$  halfway with e.g. a fast  $\pi$  pulse generated by varying the laser detuning.

Measurements of the collective spin observables are straightforward because the excited bands will have different spatial distributions upon being freed from the lattice. To measure  $\langle \hat{S}^x \rangle$  we turn off the drive and the lattice, then measure the resulting gas cloud's  $X$ -band population ( $|\uparrow\uparrow\rangle$ ) via band-mapping [28]. Measurement of  $\langle \hat{S}^y \rangle$  can be done by letting the drive run for an additional time  $t\Omega = \pi/2$  after the Ramsey protocol, rotating  $y$  into  $x$ , then repeating the  $\langle \hat{S}^x \rangle$  measurement. While  $\langle \hat{S}^z \rangle$  is in principle conserved, we can also measure it by advancing the relative phase of the Bragg beams ahead by  $\pi/2$ , which allows us to use the drive for a  $\pi/2$  pulse that rotates  $z$  into  $x$ , and then measuring  $\langle \hat{S}^x \rangle$  once more.

*Spin model validity.* Figure 2(b) benchmarks our spin model by comparing its contrast decay to that of the Fermi-Hubbard model plus drive through a root mean square error. The spin model is valid when either the lattice depth is very shallow and thus single-particle tunneling rapidly depolarizes the gas, or in the regime where the drive is strong enough to make the single particle dispersion subdominant with respect to the p-wave exchange interactions. At this point a many-body gap energetically suppresses single-particle dephasing and keeps the spins aligned. Evolution snapshots highlighting the dynamical behaviour crossover are also shown.

In the gap protected regime the dominant spin model terms are the Heisenberg term  $-\frac{U_{\uparrow\downarrow}}{4L} \sum_{\vec{k},\vec{k}'} \vec{\sigma}_{\vec{k}} \cdot \vec{\sigma}_{\vec{k}'}$  and the drive  $\frac{\Omega}{2} \sum_{\vec{k}} \hat{\sigma}_{\vec{k}}^z$ . Both these terms conserve the total spin  $S$ , defined as

$$\left[ (\hat{S}^x)^2 + (\hat{S}^y)^2 + (\hat{S}^z)^2 \right] |S, M\rangle = S(S+1) |S, M\rangle, \quad (12)$$

where  $|S, M\rangle$  are collective-spin eigenstates with non-negative  $S \in \frac{L}{2}, \frac{L}{2} - 1, \dots$  and projection  $M \in S, S-1, \dots, -S$  (satisfying  $\hat{S}^z |S, M\rangle = M |S, M\rangle$ ). An initial state in the fully-symmetric Dicke manifold ( $S = L/2$ ) will be confined to that manifold, as transitions to states with  $S < L/2$  induced by the single-particle dispersion will be

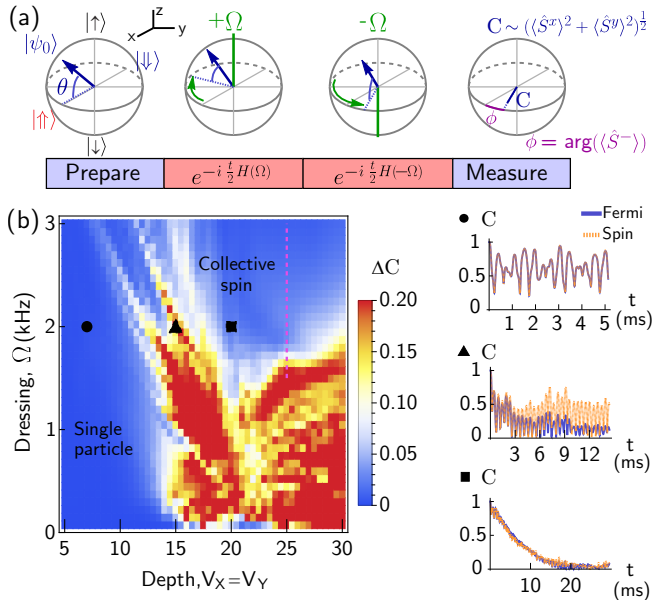


FIG. 2. (a) Schematic of Ramsey spectroscopy to measure collective spin precession, flipping the sign of  $\Omega$  at the middle of the free evolution to undo its single-particle rotation. (b) Benchmarking of spin model  $\hat{H}_S$  compared to the Fermi-Hubbard+drive  $\hat{H}_{\text{FH}} + \hat{H}_\Omega$ . Both models are evolved from a product state with  $\theta = 0$  to a time  $t_f = 50/J_1$ , and their contrast  $C$  is compared with a root-mean-square error  $\Delta C = (\frac{1}{t_f} \int_0^{t_f} dt | \frac{2}{L} (C_S - C_{\text{FH}+\Omega}) |^2 )^{1/2}$ , truncated to  $\min(\Delta C, 0.2)$  for clarity, using a small system  $L = 3 \times 2$ . Snapshots of the contrast evolution at different points in parameter space are shown on the right. The purple dashed line indicates the parameter regime explored further in Fig. 3.

energetically suppressed by the many-body gap [25, 29, 30]. This permits us to approximate the Hamiltonian by projecting it into the Dicke manifold (Supplemental Material D [26]) yielding  $\hat{H}_S \approx \hat{H}_{\text{OAT}}$ , where

$$\hat{H}_{\text{OAT}} = -\frac{U_{\uparrow\downarrow}}{L} \vec{S} \cdot \vec{S} + \chi \hat{S}^z \hat{S}^z + \Omega \hat{S}^z. \quad (13)$$

This is a one-axis twisting (OAT) model, which is well studied for its entanglement generation in the form of spin squeezing [31]. The coefficient  $\chi$  is

$$\chi = \frac{1}{L-1} \frac{2(J_0 + J_1)^2 U_{\uparrow\downarrow}}{\Omega^2 - U_{\uparrow\downarrow}^2} - \frac{1}{L} (V_{ee} - 2V_{\uparrow\downarrow}). \quad (14)$$

The first term comes from the tunneling, and the second from the cross-site interactions. Fig. 3(a) demonstrates that the contrast decay is well captured by the OAT model in addition to the preceding spin model.

While contrast decay alone can be challenging to distinguish from incoherent losses, we can also measure the collective interactions through the phase shift  $\phi$ . At the mean-field level, under the OAT model the collective spin rotates about the  $z$  axis of the Bloch sphere at a rate depending on  $\chi$  and  $\theta$ ,

$$\langle \hat{S}^- \rangle = \frac{L}{2} e^{i\phi(t)}, \quad \phi(t) = 2\chi \langle \hat{S}^z \rangle t = \chi L \sin(\theta) t, \quad (15)$$

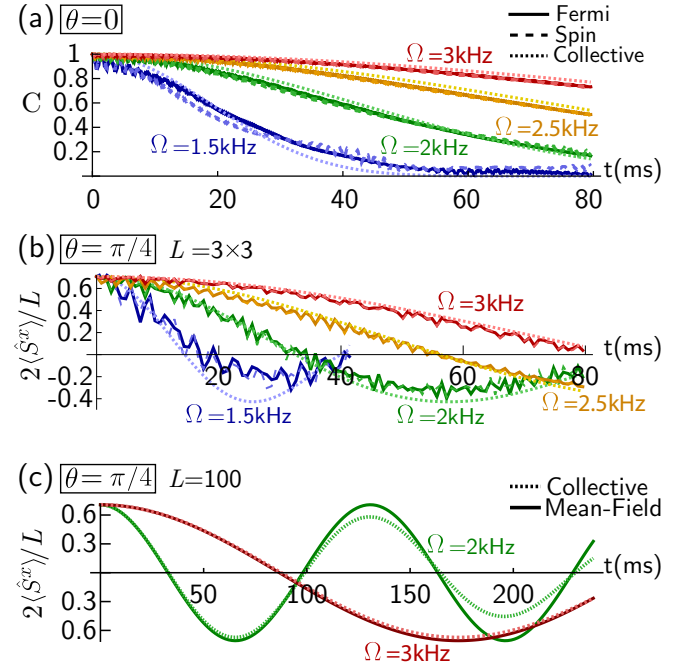


FIG. 3. (a) Time evolution of contrast decay for the Fermi-Hubbard model+drive,  $\hat{H}_{\text{FH}} + \hat{H}_\Omega$ , spin model  $\hat{H}_S$  and one-axis twisting model  $\hat{H}_{\text{OAT}}$ , for system size  $L = 3 \times 3$  and inclination angle  $\theta = \pi/4$ . The parameters used lie along the purple dashed line in the previous Fig. 2(b). (b) Time-evolution of  $\langle \hat{S}^x \rangle = C \cos(\phi)$  to measure the density phase shift  $\phi$ . (c) Time-evolution of  $\langle \hat{S}^x \rangle$  for a larger system of  $L = 100$ , using only the collective model together with its predicted mean-field behaviour.

where  $\langle \hat{S}^z \rangle = \frac{L}{2} \sin(\theta)$  is conserved. Fig. 3(b) shows sample time-evolutions of  $\langle \hat{S}^x \rangle = \text{Re}[\langle \hat{S}^- \rangle]$  with a tilt angle  $\theta = \pi/4$  for both the OAT and the underlying Fermi-Hubbard and spin models. We see an oscillation with period set by  $2\chi \langle \hat{S}^z \rangle$ . In Fig. 3(c) we show the same dynamics for a larger system using only the OAT. The frequency of the oscillations is not very sensitive to system size since  $\chi \sim 1/L$  and  $\langle \hat{S}^z \rangle \sim L$ . On the other hand, since the contrast decays more slowly with increasing  $L$ , better visibility of the oscillations is possible in larger systems.

*Conclusions and Outlook.* We have shown a robust and experimentally-realistic protocol for observing long-sought p-wave physics in optical lattices. Our specific band configuration and laser dressing allows one to isolate the interaction dynamics via collective enhancement, and see a signal on realistic timescales without the usual challenges of band relaxation or losses due to strong Feshbach resonance. The system can be reduced to a simple one-axis twisting model described by a single interaction parameter  $\chi$ , which is straightforward to measure while capturing the dominant many-body p-wave effects.

While in this work we focus on simple dynamics via mean-field Ramsey spectroscopy, well controlled spin interactions such as the OAT provide avenues to useful many-body entanglement generation and non-equilibrium quantum simula-

tion. Further progress can also realize more complex and interesting extended Fermi-Hubbard models [32] that are theoretically challenging, and yet straightforward to implement in experiment using extensions of our basic scheme. Exploration of non-collective physics such as pairing, the effects of vacancies, or local quantum correlations, can also be done with this system since tools such as quantum gas microscopes

have already been implemented in several state-of-the-art optical lattice experiments [33–37].

**Acknowledgements.** We thank Leo Radzhovsky and John Bohn for their useful feedback and careful reading of our manuscript. This work is supported by the AFOSR grants FA9550-19-1-0275, FA9550-19-1-7044, and FA9550-19-1-0365, by ARO W911NF-15-1-0603, by NSERC, by the NSF JILA-PFC PHY-1734006 grant, by NIST, and by NSERC.

---

\* mikhail.mamaev@colorado.edu

[1] C. Gross and I. Bloch, *Science* **357**, 995 (2017).

[2] F. Schäfer, T. Fukuhara, S. Sugawa, Y. Takasu, and Y. Takahashi, *Nat. Rev. Phys.* **2**, 411 (2020).

[3] V. Gurarie, L. Radzhovsky, and A. Andreev, *Phys. Rev. Lett.* **94**, 230403 (2005).

[4] V. Gurarie and L. Radzhovsky, *Ann. Phys.* **322**, 2 (2007).

[5] S. R. Elliott and M. Franz, *Rev. Mod. Phys.* **87**, 137 (2015).

[6] N. Read and D. Green, *Phys. Rev. B* **61**, 10267 (2000).

[7] J. Levinsen, N. R. Cooper, and V. Gurarie, *Phys. Rev. Lett.* **99**, 210402 (2007).

[8] H.-Y. Hui, P. Brydon, J. D. Sau, S. Tewari, and S. D. Sarma, *Sci. Rep.* **5**, 8880 (2015).

[9] Y. Jiang, D. V. Kurlov, X.-W. Guan, F. Schreck, and G. V. Shlyapnikov, *Phys. Rev. A* **94**, 011601 (2016).

[10] C. Noh and D. G. Angelakis, *Rep. Prog. Phys.* **80**, 016401 (2016).

[11] Y. Tokura and N. Nagaosa, *Science* **288**, 462 (2000).

[12] P. Coleman, “Heavy fermions: Electrons at the edge of magnetism,” in *Handbook of Magnetism and Advanced Magnetic Materials* (2007).

[13] M. A. Ruderman and C. Kittel, *Phys. Rev.* **96**, 99 (1954).

[14] M. Imada, A. Fujimori, and Y. Tokura, *Rev. Mod. Phys.* **70**, 1039 (1998).

[15] G. Khaliullin, *Progress of Theoretical Physics Supplement* **160**, 155 (2005).

[16] M. Martin, M. Bishop, M. Swallows, X. Zhang, C. Benko, J. Von-Stecher, A. Gorshkov, A. Rey, and J. Ye, *Science* **341**, 632 (2013).

[17] B. DeMarco, J. L. Bohn, J. P. Burke, M. Holland, and D. S. Jin, *Phys. Rev. Lett.* **82**, 4208 (1999).

[18] C. A. Regal, C. Ticknor, J. L. Bohn, and D. S. Jin, *Phys. Rev. Lett.* **90**, 053201 (2003).

[19] C. Luciuk, S. Trotzky, S. Smale, Z. Yu, S. Zhang, and J. H. Thywissen, *Nat. Phys.* **12**, 599 (2016).

[20] I. B. Spielman, P. R. Johnson, J. H. Huckans, C. D. Fertig, S. L. Rolston, W. D. Phillips, and J. V. Porto, *Phys. Rev. A* **73**, 020702 (2006).

[21] T. Müller, S. Fölling, A. Widera, and I. Bloch, *Phys. Rev. Lett.* **99**, 200405 (2007).

[22] G. Wirth, M. Ölschläger, and A. Hemmerich, *Nat. Phys.* **7**, 147 (2011).

[23] T. Kock, M. Ölschläger, A. Ewerbeck, W.-M. Huang, L. Mathey, and A. Hemmerich, *Phys. Rev. Lett.* **114**, 115301 (2015).

[24] M. Di Liberto, A. Hemmerich, and C. Morais Smith, *Phys. Rev. Lett.* **117**, 163001 (2016).

[25] A. Rey, L. Jiang, M. Fleischhauer, E. Demler, and M. Lukin, *Phys. Rev. A* **77**, 052305 (2008).

[26] See Supplmental Material at [hyperlink to be provided] for Notes A through D, and Figures S1 through S4.

[27] S. Baier, M. J. Mark, D. Petter, K. Aikawa, L. Chomaz, Z. Cai, M. Baranov, P. Zoller, and F. Ferlaino, *Science* **352**, 201 (2016).

[28] M. Köhl, H. Moritz, T. Stöferle, K. Günter, and T. Esslinger, *Phys. Rev. Lett.* **94**, 080403 (2005).

[29] S. Smale, P. He, B. A. Olsen, K. G. Jackson, H. Sharum, S. Trotzky, J. Marino, A. M. Rey, and J. H. Thywissen, *Science Adv.* **5**, eaax1568 (2019).

[30] A. Chu, J. Will, J. Arlt, C. Klemp, and A. M. Rey, *Phys. Rev. Lett.* **125**, 240504 (2020).

[31] M. Kitagawa and M. Ueda, *Phys. Rev. A* **47**, 5138 (1993).

[32] O. Dutta, M. Gajda, P. Hauke, M. Lewenstein, D.-S. Lühmann, B. A. Malomed, T. Sowiński, and J. Zakrzewski, *Rep. Prog. Phys.* **78**, 066001 (2015).

[33] M. F. Parsons, F. Huber, A. Mazurenko, C. S. Chiu, W. Setiawan, K. Wooley-Brown, S. Blatt, and M. Greiner, *Phys. Rev. Lett.* **114**, 213002 (2015).

[34] E. Haller, J. Hudson, A. Kelly, D. A. Cotta, B. Peaudecerf, G. D. Bruce, and S. Kuhr, *Nat. Phys.* **11**, 738 (2015).

[35] L. W. Cheuk, M. A. Nichols, M. Okan, T. Gersdorf, V. V. Ramalesh, W. S. Bakr, T. Lompe, and M. W. Zwierlein, *Phys. Rev. Lett.* **114**, 193001 (2015).

[36] A. Omran, M. Boll, T. A. Hilker, K. Kleinlein, G. Salomon, I. Bloch, and C. Gross, *Phys. Rev. Lett.* **115**, 263001 (2015).

[37] G. J. Edge, R. Anderson, D. Jervis, D. C. McKay, R. Day, S. Trotzky, and J. H. Thywissen, *Phys. Rev. A* **92**, 063406 (2015).

[38] L. Pricoupenko, *Phys. Rev. Lett.* **96**, 050401 (2006).

[39] Z. Idziaszek and T. Calarco, *Phys. Rev. Lett.* **96**, 013201 (2006).

[40] Z. Idziaszek, *Phys. Rev. A* **79**, 062701 (2009).

[41] N. T. Zinner, *Journal of Physics A: Mathematical and Theoretical* **45**, 205302 (2012).

[42] M. D. Swallows, M. Bishop, Y. Lin, S. Blatt, M. J. Martin, A. M. Rey, and J. Ye, *Science* **331**, 1043 (2011).

[43] C. S. Chiu, G. Ji, A. Mazurenko, D. Greif, and M. Greiner, *Phys. Rev. Lett.* **120**, 243201 (2018).

# Supplemental Material

## A. P-WAVE FERMI-HUBBARD MODEL DERIVATION

### A.1. Separable p-wave lattice interaction coefficients

In this appendix we show the derivation of the explicit p-wave Fermi-Hubbard terms in Eqs. (4), (5). We start by writing the interactions in real space as

$$\hat{H}_{\text{int}} = \frac{3\pi\hbar^2 b_{XY}^3}{2m} \int d^3\vec{R} \left[ \vec{\nabla}\hat{\psi}^\dagger(\vec{R}) \cdot \hat{\psi}^\dagger(\vec{R}) - \hat{\psi}^\dagger(\vec{R}) \cdot \vec{\nabla}\hat{\psi}^\dagger(\vec{R}) \right] \cdot \left[ \hat{\psi}(\vec{R}) \cdot \vec{\nabla}\hat{\psi}(\vec{R}) - \vec{\nabla}\hat{\psi}(\vec{R}) \cdot \hat{\psi}(\vec{R}) \right], \quad (\text{A1})$$

where we have used a pseudo-potential approximation, and assumed that the Feshbach field is pointed along the  $Z$  direction so that only one transverse scattering volume  $b_{XY}^3$  is relevant for interactions within each  $X$ - $Y$  lattice plane. As discussed in Refs. [38–41], when the energy-dependent scattering volume is used, the pseudo-potential gives the correct on-site eigenenergy. We consider here the perturbative-shift regime  $b_{XY}^3 \ll \ell_{\text{ho},z}^3$ , with  $\ell_{\text{ho},z}^2 = \hbar/(m\omega)$  where  $\hbar\omega = E_{\text{gap}}$  is the band gap, in which the interaction shift is small compared to the band gap  $E_{\text{gap}}$ , and linearly proportional to  $b_{XY}^3$ . These interactions can be re-written in the basis of lattice Wannier functions:

$$\hat{\psi}(\vec{R}) = \sum_{\vec{\mu}} \hat{c}_{\vec{\mu}} \phi_{\vec{\mu}}(\vec{R}), \quad (\text{A2})$$

where  $\vec{\mu} = (i, j, \gamma)$  encapsulates both a 2D lattice site index  $(i, j) = \vec{r}$  (written with two indices here for clarity) and a band index  $\gamma \in \{g, \uparrow, \downarrow\}$ . The operator  $\hat{c}_{\vec{\mu}}$  annihilates a fermion on site  $(i, j)$  in band  $\gamma$ , while  $\phi_{\vec{\mu}}(\vec{R})$  is the spatial wavefunction of band  $\gamma$  centered on that site. Assuming a separable 3D optical lattice potential, the spatial wavefunction can also be written as a product of Wannier functions  $\phi_{\vec{\mu}}(\vec{R}) = w_{n_{\vec{\mu}}^X}^X(X)w_{n_{\vec{\mu}}^Y}^Y(Y)w_{n_{\vec{\mu}}^Z}^Z(Z)$ . For example if  $\gamma = \uparrow$ , we have motional excitations of  $(n_{\vec{\mu}}^X, n_{\vec{\mu}}^Y, n_{\vec{\mu}}^Z) = (1, 0, 0)$ . Armed with these definitions, we write the interaction as

$$\begin{aligned} \hat{H}_{\text{int}} &= \sum_{\vec{\mu}_a, \vec{\mu}_b, \vec{\mu}_c, \vec{\mu}_d} U_{\vec{\mu}_a, \vec{\mu}_b, \vec{\mu}_c, \vec{\mu}_d} \hat{c}_{\vec{\mu}_a}^\dagger \hat{c}_{\vec{\mu}_b}^\dagger \hat{c}_{\vec{\mu}_c} \hat{c}_{\vec{\mu}_d}, \\ U_{\vec{\mu}_a, \vec{\mu}_b, \vec{\mu}_c, \vec{\mu}_d} &= \frac{3\pi\hbar^2 b_{XY}^3}{2m} \int d^3\vec{R} \left[ \vec{\nabla}\phi_{\vec{\mu}_a}^*(\vec{R}) \cdot \phi_{\vec{\mu}_b}^*(\vec{R}) - \phi_{\vec{\mu}_a}^*(\vec{R}) \cdot \vec{\nabla}\phi_{\vec{\mu}_b}^*(\vec{R}) \right] \cdot \left[ \phi_{\vec{\mu}_c}(\vec{R}) \cdot \vec{\nabla}\phi_{\vec{\mu}_d}(\vec{R}) - \vec{\nabla}\phi_{\vec{\mu}_c}(\vec{R}) \cdot \phi_{\vec{\mu}_d}(\vec{R}) \right], \end{aligned} \quad (\text{A3})$$

where  $\vec{\mu}_a, \vec{\mu}_b, \vec{\mu}_c, \vec{\mu}_d$  each index over all included bands and all lattice sites. Since the spatial wavefunctions are separable, the integral can also be split into cartesian components,

$$U_{\vec{\mu}_a, \vec{\mu}_b, \vec{\mu}_c, \vec{\mu}_d} = \frac{3\pi\hbar^2 b_{XY}^3}{2m} (P^X S^Y S^Z + S^X P^Y S^Z + S^X S^Y P^Z), \quad (\text{A4})$$

with the  $S$  and  $P$  integrals defined as follows (using a gauge where all Wannier functions are real-valued):

$$\begin{aligned} S^\nu &= \int_{-\infty}^{\infty} d\tilde{\nu} w_{n_{\vec{\mu}_a}^\nu}^\nu(\tilde{\nu}) w_{n_{\vec{\mu}_b}^\nu}^\nu(\tilde{\nu}) w_{n_{\vec{\mu}_c}^\nu}^\nu(\tilde{\nu}) w_{n_{\vec{\mu}_d}^\nu}^\nu(\tilde{\nu}), \\ P^\nu &= \int_{-\infty}^{\infty} d\tilde{\nu} \left[ \nabla_{\tilde{\nu}} w_{n_{\vec{\mu}_a}^\nu}^\nu(\tilde{\nu}) \cdot w_{n_{\vec{\mu}_b}^\nu}^\nu(\tilde{\nu}) - w_{n_{\vec{\mu}_a}^\nu}^\nu(\tilde{\nu}) \cdot \nabla_{\tilde{\nu}} w_{n_{\vec{\mu}_b}^\nu}^\nu(\tilde{\nu}) \right] \left[ w_{n_{\vec{\mu}_c}^\nu}^\nu(\tilde{\nu}) \cdot \nabla_{\tilde{\nu}} w_{n_{\vec{\mu}_d}^\nu}^\nu(\tilde{\nu}) - \nabla_{\tilde{\nu}} w_{n_{\vec{\mu}_c}^\nu}^\nu(\tilde{\nu}) \cdot w_{n_{\vec{\mu}_d}^\nu}^\nu(\tilde{\nu}) \right], \end{aligned} \quad (\text{A5})$$

with  $\nabla_{\tilde{\nu}}$  the derivative with respect to  $\tilde{\nu}$ .

### A.2. On-site p-wave interactions

The on-site interaction terms  $\hat{H}_{\text{int}}^{(\text{OS})}$  consist of all terms where all four  $\vec{\mu}_a, \vec{\mu}_b, \vec{\mu}_c, \vec{\mu}_d$  have the same lattice site index  $(i, j)$ . All such terms with non-vanishing matrix elements are

$$\hat{H}_{\text{int}}^{(\text{OS})} = \sum_{i,j} [U_{g\uparrow} \hat{n}_{i,j,g} \hat{n}_{i,j,\uparrow} + U_{g\downarrow} \hat{n}_{i,j,g} \hat{n}_{i,j,\downarrow} + U_{\uparrow\downarrow} \hat{n}_{i,j,\uparrow} \hat{n}_{i,j,\downarrow}]. \quad (\text{A6})$$

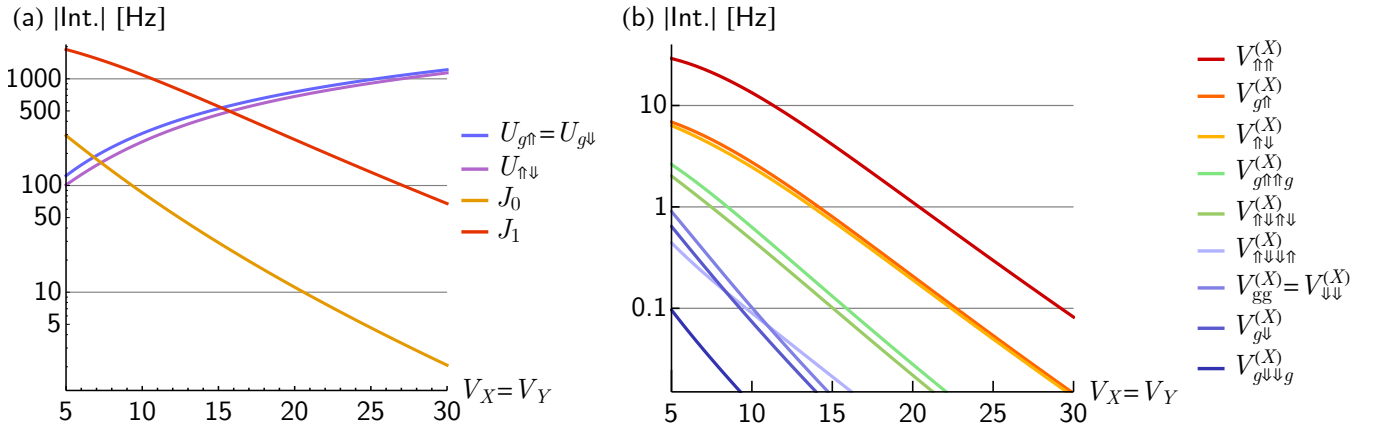


FIG. S1. (a) On-site interaction parameter and lattice tunneling rate magnitudes as a function of  $V_X = V_Y$  lattice depth in units of recoil energy. Transverse lattice depth is fixed at  $V_Z = 100$ , and scattering length set to  $b_{XY} = 292a_0$ . Overlap integrals are computed using ideal Wannier functions. (b) Nearest-neighbour interaction parameters along the  $X$ -direction. The  $V_{\uparrow\uparrow}^{(X)}$ ,  $V_{g\uparrow\uparrow}^{(X)}$ ,  $V_{\uparrow\downarrow}^{(X)}$  terms are strongest, and we will neglect all others.

Here  $U_{g\uparrow\uparrow}$ ,  $U_{g\downarrow\downarrow}$  and  $U_{\uparrow\downarrow}$  are specific interaction parameters coming from spatial overlap integrals defined above. For clarity, we will first work out which interaction coefficients are relevant to the model, and then show the explicit integral expressions for them at the end of the derivation. Fig. S1(a) shows a numerical comparison of these interaction strength magnitudes together with the tunneling rates  $J_0$ ,  $J_1$  as a function of the lattice depths  $V_X = V_Y$  (fixing  $V_Z = 100$  and  $b_{XY} = 292a_0$  as in the main text). Naturally, the on-site interaction strengths increase with tighter confinement while the tunneling decreases exponentially.

### A.3. Cross-site p-wave interactions

The next set of terms is the cross-site interactions, for which the spatial index  $\vec{r} = (i, j)$  is not the same for all four operators. Before writing them down, we first identify several types of terms which are *not* going to be included. We neglect all of the following:

- Any terms that do not conserve the fixed population of two atoms per lattice site, such as paired hops  $\hat{c}_{i,j,\uparrow}^\dagger \hat{c}_{i,j,\downarrow}^\dagger \hat{c}_{i+1,j,\uparrow} \hat{c}_{i+1,j,\downarrow}$  or interaction-assisted tunneling  $\hat{n}_{i,j,\uparrow} (\hat{c}_{i,j,\downarrow}^\dagger \hat{c}_{i+1,j,\downarrow} + h.c.)$ . Such terms are energetically suppressed by the stronger on-site interactions provided that the lattice is not too shallow.
- Terms that move atoms in/out of the ground band  $|g\rangle$ , such as interaction-assisted flips  $\hat{n}_{i,j,\uparrow} (\hat{c}_{i+1,j,\downarrow}^\dagger \hat{c}_{i+1,j,g} + h.c.)$  or double-flips  $\hat{c}_{i,j,\uparrow}^\dagger \hat{c}_{i,j,g} \hat{c}_{i+1,j,\uparrow}^\dagger \hat{c}_{i+1,j,g}$ . These are suppressed by the band gap.
- Any terms that are further range than nearest-neighbour. These are suppressed by exponential falloff of the Wannier functions provided that the lattice is not too shallow.

The remaining non-neglected cross-site interactions can be written as

$$\hat{H}_{\text{int}}^{(\text{CS})} = \hat{H}_{\text{int}}^{(\text{CS},X)} + \hat{H}_{\text{int}}^{(\text{CS},Y)}, \quad (\text{A7})$$

where  $\hat{H}_{\text{int}}^{(\text{CS},X)}$  ( $\hat{H}_{\text{int}}^{(\text{CS},Y)}$ ) are the terms along the nearest neighbour  $X$  ( $Y$ ) direction respectively. For example along  $X$  the non-vanishing, non-neglected terms are

$$\begin{aligned} \hat{H}_{\text{int}}^{(\text{CS},X)} = & V_{gg}^{(X)} \sum_{i,j} \hat{n}_{i,j,g} \hat{n}_{i+1,j,g} + V_{\uparrow\uparrow}^{(X)} \sum_{i,j} \hat{n}_{i,j,\uparrow} \hat{n}_{i+1,j,\uparrow} + V_{\downarrow\downarrow}^{(X)} \sum_{i,j} \hat{n}_{i,j,\downarrow} \hat{n}_{i+1,j,\downarrow} \\ & + V_{g\uparrow\uparrow}^{(X)} \sum_{i,j} (\hat{n}_{i,j,g} \hat{n}_{i+1,j,\uparrow} + \hat{n}_{i,j,\uparrow} \hat{n}_{i+1,j,g}) + V_{g\downarrow\downarrow}^{(X)} \sum_{i,j} (\hat{n}_{i,j,g} \hat{n}_{i+1,j,\downarrow} + \hat{n}_{i,j,\downarrow} \hat{n}_{i+1,j,g}) + V_{\uparrow\downarrow}^{(X)} \sum_{i,j} (\hat{n}_{i,j,\uparrow} \hat{n}_{i+1,j,\downarrow} + \hat{n}_{i,j,\downarrow} \hat{n}_{i+1,j,\uparrow}) \\ & + V_{\uparrow\uparrow\uparrow\uparrow}^{(X)} \sum_{i,j} (\hat{c}_{i,j,g}^\dagger \hat{c}_{i,j,\uparrow} \hat{c}_{i+1,j,\uparrow}^\dagger \hat{c}_{i+1,j,g} + h.c.) + V_{g\uparrow\uparrow\uparrow}^{(X)} \sum_{i,j} (\hat{c}_{i,j,g}^\dagger \hat{c}_{i,j,\uparrow} \hat{c}_{i+1,j,\uparrow}^\dagger \hat{c}_{i+1,j,g} + h.c.) \\ & + V_{\uparrow\uparrow\downarrow\downarrow}^{(X)} \sum_{i,j} (\hat{c}_{i,j,\uparrow}^\dagger \hat{c}_{i,j,\downarrow} \hat{c}_{i+1,j,\downarrow}^\dagger \hat{c}_{i+1,j,\uparrow} + h.c.) + V_{g\uparrow\uparrow\downarrow\downarrow}^{(X)} \sum_{i,j} (\hat{c}_{i,j,\uparrow}^\dagger \hat{c}_{i,j,\downarrow} \hat{c}_{i+1,j,\downarrow}^\dagger \hat{c}_{i+1,j,\uparrow} + h.c.). \end{aligned} \quad (\text{A8})$$

The  $Y$ -direction terms will look analogous, except with different coefficients  $V_{gg}^{(Y)}$ ,  $V_{\uparrow\uparrow}^{(Y)}$ , etc., and involving pairs of lattice sites  $(i, j)$ ,  $(i, j + 1)$  instead of  $(i, j)$ ,  $(i + 1, j)$  as above.

Fig. S1(b) shows the cross-site interaction parameters along  $X$  for all of the above terms. They all decay exponentially like the tunneling rates. Unsurprisingly, the terms involving the  $|\uparrow\rangle$  orbital have the strongest magnitudes since the  $|\uparrow\rangle$  spatial wavefunction is more delocalized along  $X$ . The  $V_{\uparrow\uparrow}^{(X)}$  term interaction of two  $|\uparrow\rangle$  atoms is the strongest, followed by interaction  $V_{g\uparrow}^{(X)}$  between  $|\uparrow\rangle$ ,  $|g\rangle$  atoms and interaction  $V_{\uparrow\downarrow}^{(X)}$  between  $|\uparrow\rangle$ ,  $|\downarrow\rangle$  atoms. All of the other terms are smaller by about an order of magnitude, and we neglect them. For the  $Y$ -direction interactions, we analogously keep only the strongest terms, which will involve the  $|\downarrow\rangle$  orbital atoms instead. We are left with

$$\begin{aligned} \hat{H}_{\text{int}}^{(\text{CS})} \approx & \sum_{i,j} \left[ V_{\uparrow\uparrow}^{(X)} \hat{n}_{i,j,\uparrow} \hat{n}_{i+1,j,\uparrow} + V_{\uparrow\downarrow}^{(X)} (\hat{n}_{i,j,\uparrow} \hat{n}_{i+1,j,\downarrow} + \hat{n}_{i,j,\downarrow} \hat{n}_{i+1,j,\uparrow}) + V_{g\uparrow}^{(X)} (\hat{n}_{i,j,g} \hat{n}_{i+1,j,\uparrow} + \hat{n}_{i,j,\uparrow} \hat{n}_{i+1,j,g}) \right] \\ & + \sum_{i,j} \left[ V_{\downarrow\downarrow}^{(Y)} \hat{n}_{i,j,\downarrow} \hat{n}_{i+1,j,\downarrow} + V_{\uparrow\downarrow}^{(Y)} (\hat{n}_{i,j,\uparrow} \hat{n}_{i+1,j,\downarrow} + \hat{n}_{i,j,\downarrow} \hat{n}_{i+1,j,\uparrow}) + V_{g\downarrow}^{(Y)} (\hat{n}_{i,j,g} \hat{n}_{i+1,j,\downarrow} + \hat{n}_{i,j,\downarrow} \hat{n}_{i+1,j,g}) \right]. \end{aligned} \quad (\text{A9})$$

#### A.4. Frozen ground band approximation

Since we assume that the ground band  $|g\rangle$  is completely filled, we can simplify any terms involving  $|g\rangle$  atoms. The ground band atoms cannot tunnel due to Pauli exclusion as they are spin-polarized. Furthermore, there are no energy-conserving p-wave interaction processes that can kick them out of the band due to the band gap. We can assume that all  $|g\rangle$  atoms will simply sit in place throughout the system's time-evolution, which amounts to

$$\hat{c}_{i,j,g}^\dagger \hat{c}_{i',j',g} = \delta_{i,i'} \delta_{j,j'} \mathbb{1}. \quad (\text{A10})$$

Applying this approximation to the interactions allows us to drop the terms involving  $|g\rangle$  atoms entirely, because they amount to constant shifts to the Hamiltonian. In the on-site terms  $\hat{H}_{\text{int}}^{(\text{OS})}$  we have

$$\sum_{i,j} (U_{g\uparrow} \hat{n}_{i,j,g} \hat{n}_{i,j,\uparrow} + U_{g\downarrow} \hat{n}_{i,j,g} \hat{n}_{i,j,\downarrow}) = \sum_{i,j} (U_{g\uparrow} \hat{n}_{i,j,\uparrow} + U_{g\downarrow} \hat{n}_{i,j,\downarrow}) \sim \sum_{i,j} (\hat{n}_{i,j,\uparrow} + \hat{n}_{i,j,\downarrow}) \sim L \mathbb{1}, \quad (\text{A11})$$

because  $U_{g\uparrow} = U_{g\downarrow}$  for equal lattice depths  $V_X = V_Y$ , and the total atom number  $\sum_{i,j} (\hat{n}_{i,j,\uparrow} + \hat{n}_{i,j,\downarrow})$  is conserved assuming we have no band relaxation. In the cross-site interactions  $\hat{H}_{\text{int}}^{(\text{CS})}$  we have

$$\begin{aligned} \sum_{i,j} \left[ V_{g\uparrow}^{(X)} (\hat{n}_{i,j,g} \hat{n}_{i+1,j,\uparrow} + \hat{n}_{i,j,\uparrow} \hat{n}_{i+1,j,g}) + V_{g\downarrow}^{(Y)} (\hat{n}_{i,j,g} \hat{n}_{i+1,j,\downarrow} + \hat{n}_{i,j,\downarrow} \hat{n}_{i+1,j,g}) \right] &= 2 \sum_{i,j} \left( V_{g\uparrow}^{(X)} \hat{n}_{i,j,\uparrow} + V_{g\downarrow}^{(Y)} \hat{n}_{i,j,\downarrow} \right) \\ &\sim \sum_{i,j} (\hat{n}_{i,j,\uparrow} + \hat{n}_{i,j,\downarrow}) \sim L \mathbb{1}, \end{aligned} \quad (\text{A12})$$

again because  $V_{g\uparrow}^{(X)} = V_{g\downarrow}^{(Y)}$  for equal lattice depths  $V_X = V_Y$ . Applying these reductions to  $\hat{H}_{\text{int}}^{(\text{OS})}$  and  $\hat{H}_{\text{int}}^{(\text{CS})}$ , and defining

$$V_{ee} \equiv V_{\uparrow\uparrow}^{(X)} = V_{\downarrow\downarrow}^{(Y)}, \quad V_{\uparrow\downarrow} \equiv V_{\uparrow\downarrow}^{(X)} = V_{\uparrow\downarrow}^{(Y)} \quad \text{for } V_X = V_Y \quad (\text{A13})$$

leads to the corresponding Hamiltonians in the main text.

#### A.5. Interaction parameter form

Here we give explicit integral expressions for the three interaction parameters we keep in the models, in terms of Wannier function overlaps. The on-site interaction  $U_{\uparrow\downarrow}$  is

$$\begin{aligned} U_{\uparrow\downarrow} = & \frac{6\pi\hbar^2 b_{XY}^3}{m} \left[ \int_{-\infty}^{\infty} dX \left( \frac{dw_1^X(X)}{dX} \cdot w_0^X(X) - w_1^X(X) \cdot \frac{dw_0^X(X)}{dX} \right)^2 \int_{-\infty}^{\infty} dY w_0^Y(Y)^2 w_1^Y(Y)^2 \int_{-\infty}^{\infty} dZ w_0^Z(Z)^4 \right. \\ & \left. + \int_{-\infty}^{\infty} dX w_1^X(X)^2 w_0^X(X)^2 \int_{-\infty}^{\infty} dY \left( \frac{dw_1^Y(Y)}{dY} \cdot w_0^Y(Y) - w_1^Y(Y) \cdot \frac{dw_0^Y(Y)}{dY} \right)^2 \int_{-\infty}^{\infty} dZ w_0^Z(Z)^4 \right], \end{aligned} \quad (\text{A14})$$

where we have assumed a gauge where all Wannier functions are real-valued. The cross-site interaction terms  $V_{ee}$ ,  $V_{\uparrow\downarrow}$  are (using the  $X$ -direction without loss of generality)

$$\begin{aligned} V_{ee} &= \frac{6\pi\hbar^2 b_{XY}^3}{m} \cdot \int_{-\infty}^{\infty} dX \left( \frac{dw_1^X(X)}{dX} \cdot w_1^X(X-a) - w_1^X(X) \cdot \frac{dw_1^X(X-a)}{dX} \right)^2 \int_{-\infty}^{\infty} dY w_0^Y(Y)^4 \int_{-\infty}^{\infty} dZ w_0^Z(Z)^4, \\ V_{\uparrow\downarrow} &= \frac{6\pi\hbar^2 b_{XY}^3}{m} \left[ \int_{-\infty}^{\infty} dX \left( \frac{dw_1^X(X)}{dX} \cdot w_0^X(X-a) - w_1^X(X) \cdot \frac{dw_0^X(X-a)}{dX} \right)^2 \int_{-\infty}^{\infty} dY w_0^Y(Y)^2 w_1^Y(Y)^2 \int_{-\infty}^{\infty} dZ w_0^Z(Z)^4 \right. \\ &\quad \left. + \int_{-\infty}^{\infty} dX w_1^X(X)^2 w_0^X(X-a)^2 \int_{-\infty}^{\infty} dY \left( \frac{dw_1^Y(Y)}{dY} \cdot w_0^Y(Y) - w_1^Y(Y) \cdot \frac{dw_0^Y(Y)}{dY} \right)^2 \int_{-\infty}^{\infty} dZ w_0^Z(Z)^4 \right], \end{aligned} \quad (\text{A15})$$

with  $a$  the lattice spacing.

## B. LASER DRESSING AND COUPLING

### B.1. Bragg dressing

Here we detail the implementation of Bragg laser coupling between our desired band states. We write the Hamiltonian of a single lattice site in the basis of  $|\uparrow\rangle$ ,  $|\downarrow\rangle$ , together with a manifold of intermediate excited states  $\{|E\rangle\}$ . This intermediate state manifold is typically the continuum of an untrapped excited electronic state hyperfine level, separated from the ground electronic states by an optical frequency. We couple the desired band states to the intermediate excited states with two Bragg-type laser beams with single-photon Rabi frequencies  $\Omega_1, \Omega_2$  (assumed real for simplicity) and wavevectors  $\vec{k}_1, \vec{k}_2$ . Assuming that we have a large detuning  $\Delta \gg \Omega_1, \Omega_2$  from the intermediate state manifold, the second-order effective coupling between our excited band states  $|a\rangle, |b\rangle \in \{|\uparrow\rangle, |\downarrow\rangle\}$  is

$$\begin{aligned} \langle a | \hat{H}_\Omega | b \rangle \approx & -\frac{1}{4\Delta} \sum_{|E\rangle} \left[ \Omega_1^2 \langle a | e^{i\vec{k}_1 \vec{r}} | E \rangle \langle E | e^{-i\vec{k}_1 \vec{r}} | b \rangle + \Omega_1 \Omega_2 \langle a | e^{i\vec{k}_1 \vec{r}} | E \rangle \langle E | e^{-i\vec{k}_2 \vec{r}} | b \rangle \right. \\ & \left. + \Omega_2 \Omega_1 \langle a | e^{i\vec{k}_2 \vec{r}} | E \rangle \langle E | e^{-i\vec{k}_1 \vec{r}} | b \rangle + \Omega_2^2 \langle a | e^{i\vec{k}_2 \vec{r}} | E \rangle \langle E | e^{-i\vec{k}_2 \vec{r}} | b \rangle \right], \end{aligned} \quad (\text{B1})$$

where  $\vec{r}$  is the position vector from the center of the lattice site. This description is valid provided that the effective bandwidth of the intermediate state manifold  $\{|E\rangle\}$  is small compared to  $\Delta$ . Furthermore, under the assumption that the intermediate state is not trapped by the lattice, it acts as a continuum, allowing the approximation of

$$\sum_{|E\rangle} |E\rangle \langle E| = 1. \quad (\text{B2})$$

Our matrix elements then simplify to

$$\langle a | \hat{H}_\Omega | b \rangle \approx -\frac{1}{4\Delta} \left[ \Omega_1^2 \delta_{ab} + \Omega_1 \Omega_2 \langle a | e^{i(\vec{k}_1 - \vec{k}_2) \vec{r}} | b \rangle + \Omega_2 \Omega_1 \langle a | e^{-i(\vec{k}_1 - \vec{k}_2) \vec{r}} | b \rangle + \Omega_2^2 \delta_{ab} \right]. \quad (\text{B3})$$

The first and last term correspond to overall Stark shifts that are equal for both spin states  $|\uparrow\rangle$ ,  $|\downarrow\rangle$ , contributing no overall effect. The middle two terms will create the desired two-photon coupling between the spin states that we are after. The effective two-photon Rabi frequency will be

$$\frac{\Omega}{2} = -\frac{\Omega_1 \Omega_2}{2\Delta} \langle \uparrow | \cos(\Delta \vec{k} \cdot \vec{r}) | \downarrow \rangle, \quad (\text{B4})$$

where  $\Delta \vec{k} = \vec{k}_1 - \vec{k}_2$  is the differential momentum kick of the two laser beams.

### B.2. Elimination of cross-site effects

Thus far, we have written the Hamiltonian for a single arbitrary lattice site. In principle the position vector  $\vec{r}$  multiplying the laser wavevectors must be written using its full real-space value including the lattice site position. At a given lattice site integer index  $(i, j)$ , we have

$$\vec{r} = a(i, j, 0) + (X, Y, Z), \quad (\text{B5})$$

with  $a$  the lattice spacing and  $(X, Y, Z)$  the position from the center of the given lattice site. The cosine in the effective  $\hat{H}_\Omega$  matrix elements is then written (for a single 2D  $X$ - $Y$  lattice plane, assuming that  $\Delta\vec{k}$  has no  $Z$ -component)

$$\cos(\Delta\vec{k} \cdot \vec{r}) = \cos[\Delta\vec{k} \cdot (X, Y, Z) + a \Delta\vec{k} \cdot (i, j, 0)]. \quad (\text{B6})$$

The first term of the cosine argument is the actual spatially-varying phase across the given lattice site, which will be integrated with the on-site lattice Wannier functions of the different cartesian components  $X, Y, Z$ . The second term,

$$\eta \equiv a \Delta\vec{k} \cdot (i, j, 0), \quad (\text{B7})$$

is an additional phase that corresponds to a spin-orbit coupling effect due to the possibly incommensurate wavelengths of the lattice and drives. Evaluating our desired matrix element between  $|\uparrow\uparrow\rangle$  and  $|\downarrow\downarrow\rangle$  we get

$$\langle \uparrow\uparrow | \hat{H}_\Omega | \downarrow\downarrow \rangle = \frac{\Omega_1 \Omega_2}{2\Delta} \cos(\eta) \int_{-\infty}^{\infty} dX w_1^X(X) \sin(\Delta\vec{k}_X X) w_0^X(X) \int_{-\infty}^{\infty} dY w_0^Y(Y) \sin(\Delta\vec{k}_Y Y) w_1^Y(Y), \quad (\text{B8})$$

where  $\Delta\vec{k} = (\Delta\vec{k}_X, \Delta\vec{k}_Y, 0)$  (still assuming no momentum kick along  $Z$ ). The overall two-photon frequency  $\Omega$  gets normalized by the spin-orbit coupling phase via the  $\cos(\eta)$  prefactor that varies across different lattice sites,

$$\Omega \rightarrow \Omega \cos(\eta). \quad (\text{B9})$$

The Bragg beams effectively act as an additional lattice potential whose direction and wavelength depends on the differential momentum kick  $\Delta\vec{k}$ , only providing a coupling between motional states rather than a Stark shift.

Ideally we want to have as large and as uniform of a Rabi frequency  $\Omega$  as possible across the lattice. Making it large requires both  $\Delta\vec{k}_X$  and  $\Delta\vec{k}_Y$  to be non-zero, as otherwise the sines in the integrands above will vanish due to the Wannier functions' even/odd spatial symmetry. For example, we could use the scheme in the main text, where one beam comes in along the  $X$  direction and one along the  $Y$  direction, each co-propagating with the lattice beams,

$$\text{Example: } \vec{k}_1 = \frac{2\pi}{\lambda}(1, 0, 0), \quad \vec{k}_2 = \frac{2\pi}{\lambda}(0, -1, 0), \quad \rightarrow \quad \Delta\vec{k} = \frac{2\pi}{\lambda}(1, 1, 0), \quad (\text{B10})$$

with  $\lambda$  the wavelength of the Bragg beams. On the other hand, making the Rabi frequency uniform requires us to minimize the effect of the spin-orbit coupling phase. This can be done by making the phase as close as possible to an integer multiple of  $2\pi$ ,

$$\eta = 2\pi m, \quad m \in \mathbb{Z}, \quad (\text{B11})$$

which requires that both the  $X$  and  $Y$  directions independently satisfy

$$a\Delta\vec{k}_X = 2\pi m, \quad a\Delta\vec{k}_Y = 2\pi m', \quad m, m' \in \mathbb{Z}. \quad (\text{B12})$$

For our example, this condition amounts to

$$\text{Example: } \frac{2\pi a}{\lambda} = 2\pi m, \quad m \in \mathbb{Z}, \quad (\text{B13})$$

which can be satisfied with an appropriate choice of wavelengths and/or lattice spacing such as by choosing  $\lambda = a$ , i.e Bragg beams with half the lattice beam wavelength.

### B.3. SOC Benchmarking

We benchmark how much of a dressing laser wavelength mismatch can be tolerated while still maintaining a coherent collective-spin signal in the Ramsey spectroscopy. We assume the drive lasers to co-propagate with the  $X, Y$  lattice axes as in the example above. The wavelength mismatch is quantified by a dimensionless parameter  $\eta_0$

$$\eta_0 \equiv \frac{2\pi a}{\lambda} - 2\pi. \quad (\text{B14})$$

When  $\eta_0 = 0$ , the SOC phase is always an integer multiple of  $2\pi$  and there are no SOC modulation effects on the drive Rabi frequency  $\Omega$ . As  $\eta_0$  increases, the modulation gets stronger, and the coherence of the collective spin signal is lost. In Fig. S2 we

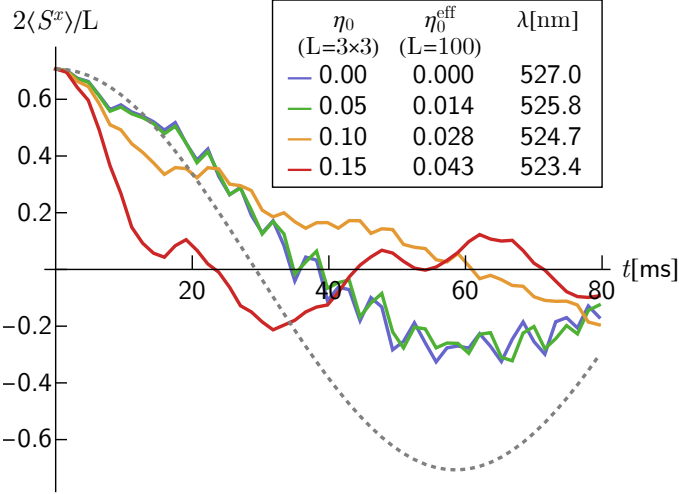


FIG. S2. Time-evolution of  $\langle \hat{S}^x \rangle$  to measure the mean-field density phase shift, under the presence of spin-orbit coupling effects. We simulate an  $L = 3 \times 3$  system using the Fermi-Hubbard model, written in real space with periodic boundary conditions, starting from a collective product state  $|\psi_0\rangle$  inclined at  $\theta = \pi/4$  as per the protocol described in the main text. The gray dashed line is the expected mean-field precession. The drive on each lattice site  $(i, j)$  is modulated by the presence of spin-orbit coupling,  $\Omega \rightarrow \Omega \cos(\eta)$  with  $\eta = \eta_0[(i - i_0) + (j - j_0)]$  [with  $(i_0, j_0)$  the center site of the lattice, here  $(2, 2)$ ]. Different color dots represent the evolution for different values of  $\eta_0$ . The legend also shows the effective  $\eta_0^{\text{eff}}$  for a larger system of size  $L = 100$ , calculated by computing the average value of  $\cos(\eta)$  for a given  $\eta_0$ , and determining what the corresponding  $\eta_0^{\text{eff}}$  would need to be to have the same average if sampling over a  $10 \times 10$  grid with it. The corresponding laser drive wavelength  $\lambda$  is also provided, assuming lattice period  $a = 527 \text{ nm}$ , and Bragg beams co-propagating with the  $X, Y$  lattice beams respectively.

show the time-evolution of the density phase via  $\langle \hat{S}^x \rangle$  for different values of  $\eta_0$ . We assume that the maximum-amplitude region is at the center of the lattice, for which we would have

$$\eta = \eta_0[(i - i_0) + (j - j_0)], \quad (\text{B15})$$

with  $(i_0, j_0)$  the central site of the lattice. The simulation uses a small system size  $L = 3 \times 3$  with periodic boundary conditions (while these are somewhat unphysical given the spatial structure  $\Omega \cos(\eta)$  of the modulation, they help avoid strong boundary effects). We see that for sufficiently small  $\eta_0$  mismatch the signal's oscillation correctly follows the mean-field envelope (up to decay of the contrast). A larger  $\eta_0$  causes the signal oscillation period to change, because there are additional perturbative contributions to the mean-field precession rate  $\chi$  that emerge. Even larger  $\eta_0$  will cause the signal to decay altogether as the gap protection keeping the system in the highest angular momentum shell breaks down.

While the modulation grows stronger for every lattice site increment away from the center, we can still estimate the maximum tolerable mismatch for a larger lattice size. A larger  $\eta_0$  for our  $L = 3 \times 3$  system simply corresponds to a smaller effective  $\eta_0^{\text{eff}}$  for a bigger system. In the legend of Fig. S2, we show what that effective  $\eta_0^{\text{eff}}$  would be for an  $L = 10 \times 10$  system, by simply computing what average value of  $\cos[\eta_0^{\text{eff}}(i - i_0 + j - j_0)]$  for  $L = 10 \times 10$  matches the average value of  $\cos[\eta_0(i - i_0 + j - j_0)]$  for  $L = 3 \times 3$ . This  $\eta_0^{\text{eff}}$  provides an estimate of what kind of mismatch a realistic experiment can tolerate assuming it traps atoms in a  $10 \times 10$  site region at the lattice center. The figure also provides the corresponding laser wavelength  $\lambda$  for lattice spacing  $a = 527 \text{ nm}$ . To have  $\eta_0^{\text{eff}} = 0$  we would need  $\lambda = a$  exactly, and we can tolerate deviations of about  $1 - 2 \text{ nm}$  away from that.

#### B.4. Other bands

Thus far, we have only included the three motional bands  $|g\rangle$  [excitation numbers  $(0, 0, 0)$ ],  $|\uparrow\rangle$   $[(1, 0, 0)]$  and  $|\downarrow\rangle$   $[(0, 1, 0)]$  in our calculations. A 3D optical lattice will have other bands such as  $(2, 0, 0)$ ,  $(0, 0, 1)$ , etc., which can still be coupled to by the drive. This sets an upper limit on how high we can make the two-photon Rabi frequency  $\Omega$ , as increasing it will also increase the unwanted couplings to other bands, which will cause the system to heat once they surpass the band-gaps.

To ensure that this does not happen in our system, we simulate the dynamics of a single lattice site starting with our standard initial condition of one atom in  $|g\rangle$  and one in  $|\uparrow\rangle$ , then including all possible other band states with up to three motional excitations. We then compute all coupling matrix elements induced by our lasers via Eq. (B4), where  $|a\rangle$ ,  $|b\rangle$  now run over all of the included band states. The wavevectors of the lasers are chosen to co-propagate with the lattice beams as in the example of Eq. (B10), with a wavelength  $\lambda = a$  to avoid any SOC effects. We include only the single-particle terms of the drive and band-gaps without the interactions, as we work in a regime where the drive is the dominant energy scale in the system.

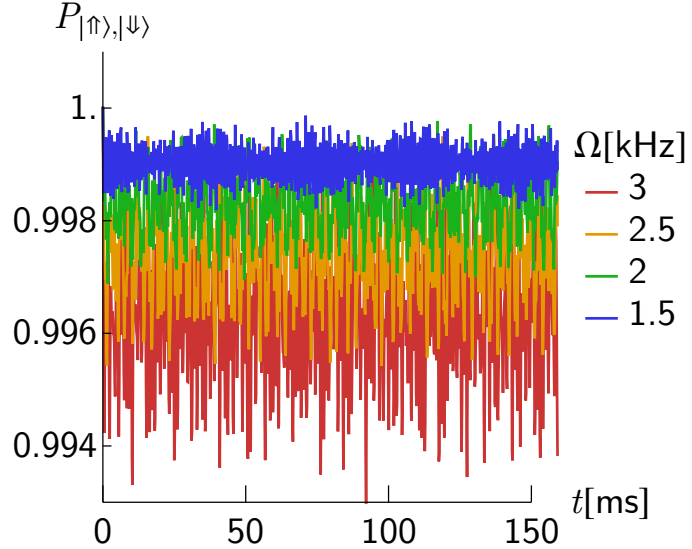


FIG. S3. Wavefunction population in the desired spin-1/2 subspace for a single lattice site evolving under the laser drive and including higher motional bands. All band states with up to 3 motional excitations are included. Only single-particle terms (the laser drive couplings and the band gaps) are used, as these are the dominant energy scales in the system.

Fig. S3 shows the dynamics of wavefunction population  $P_{|\uparrow\rangle,|\psi\rangle}$  in the manifold of our two desired spin states, thus the two Fock states both with one atom in  $|g\rangle$ , and one atom in  $|\uparrow\rangle$  or  $|\downarrow\rangle$  respectively, for different values of  $\Omega$ .

We note that a coherent Bragg laser field is advantageous for suppressing heating because it mitigates couplings to the closest-lying unwanted band states. The coupling between generic orbitals  $|a\rangle$  and  $|b\rangle$  is an extension of Eq. (B8), which can be written as (still assuming  $\Delta k_Z = 0$ )

$$\langle a | \hat{H}_\Omega | b \rangle = \frac{\Omega_1 \Omega_2}{2\Delta} \cos(\eta) \int_{-\infty}^{\infty} dX w_{n_a^X}^X(X) \sin(\Delta \vec{k}_X X) w_{n_b^X}^X(X) \int_{-\infty}^{\infty} dY w_{n_a^Y}^Y(Y) \sin(\Delta \vec{k}_Y Y) w_{n_b^Y}^Y(Y), \quad (\text{B16})$$

with  $(n_a^X, n_a^Y, n_a^Z)$  and  $(n_b^X, n_b^Y, n_b^Z)$  the orbital harmonic excitation numbers of states  $|a\rangle$  and  $|b\rangle$ . Our desired subspace consists of the states with excitations  $(1, 0, 0)$  and  $(0, 1, 0)$ . Assuming a deeper lattice along  $Z$ , the other closest-lying band states are  $(0, 0, 0)$  (the ground band),  $(2, 0, 0)$ ,  $(0, 2, 0)$  and  $(1, 1, 0)$  (doubly-excited  $X, Y$  bands). For all of these, the above coupling to  $(1, 0, 0)$  and  $(0, 1, 0)$  will vanish due to spatial parity. The only way population can leak is through couplings to triply-excited states or above, such as  $(3, 0, 0)$ . The energy gap to these is twice the band-gap, which permits a larger value of  $\Omega$  without significant population loss.

### C. SPIN MODEL DERIVATION USING NO-MODE-CHANGING-COLLISIONS APPROXIMATION

#### C.1. Absence of mode-changing collisions

Here we show how the Fermi-Hubbard model together with the laser drive ( $\hat{H}_{\text{FH}} + \hat{H}_\Omega$ ) can be approximated with a spin model using a no-mode-changing-collisions approximation.

Any quadratic terms such as the tunneling or drive can be directly written as effective spin rotations. We first focus on the interactions instead. As a demonstrative example, we show how the nearest-neighbour attraction of two  $|\uparrow\rangle$  atoms is transformed into a spin term. We work in the non-dressed basis  $\{\hat{c}_{i,j,\uparrow}, \hat{c}_{i,j,\downarrow}\}$  with two spatial indices  $(i, j) = \vec{r}$ , and convert to the dressed basis at the end. The corresponding Fermi-Hubbard term can be written as

$$I_{\uparrow\uparrow} = V_{ee} \sum_{i,j} \hat{n}_{i,j,\uparrow} \hat{n}_{i+1,j,\uparrow} = \frac{V_{ee}}{L} \sum_{k_X, k'_X, q_X} \sum_{k_Y, k'_Y, q_Y} e^{-i(k_X - k'_X + q_X)} \hat{c}_{k_X + q_X, k_Y + q_Y, \uparrow}^\dagger \hat{c}_{k'_X, k'_Y, \uparrow}^\dagger \hat{c}_{k'_X - q_X, k'_Y - q_Y, \uparrow}^\dagger \hat{c}_{k_X, k_Y, \uparrow}, \quad (\text{C1})$$

where  $k_X, k'_X, q_X$  and  $k_Y, k'_Y, q_Y$  are 2D quasimomenta along  $X$  and  $Y$  lattice directions respectively. The no-mode-changing-collisions approximation amounts to only keeping those terms of the sums that conserve individual quasimomentum mode

population,

$$\hat{c}_{\vec{k}_1,\uparrow}^\dagger \hat{c}_{\vec{k}_2,\uparrow} \hat{c}_{\vec{k}_3,\uparrow}^\dagger \hat{c}_{\vec{k}_4,\uparrow} = 0 \quad \text{unless } \vec{k}_1 = \vec{k}_2, \vec{k}_3 = \vec{k}_4 \text{ or } \vec{k}_1 = \vec{k}_4, \vec{k}_2 = \vec{k}_3. \quad (\text{C2})$$

Applying this approximation leaves the following terms:

$$I_{\uparrow\uparrow} = \frac{V_{ee}}{L} \sum_{\vec{k}, \vec{k}'} e^{-i(k_X - k'_X)} \hat{c}_{\vec{k},\uparrow}^\dagger \hat{c}_{\vec{k}',\uparrow} \hat{c}_{\vec{k}',\uparrow}^\dagger \hat{c}_{\vec{k},\uparrow} + \frac{V_{ee}}{L} \sum_{\vec{k} \neq \vec{k}'} \hat{c}_{\vec{k},\uparrow}^\dagger \hat{c}_{\vec{k},\uparrow} \hat{c}_{\vec{k}',\uparrow}^\dagger \hat{c}_{\vec{k}',\uparrow}, \quad (\text{C3})$$

using indices  $\vec{k} = (k_X, k_Y)$ ,  $\vec{k}' = (k'_X, k'_Y)$  in this equation and hereafter.

### C.2. Spin model mapping

We now commute the operators and map them to spin-1/2 operators via

$$\hat{c}_{\vec{k},\uparrow}^\dagger \hat{c}_{\vec{k},\downarrow} = \hat{\sigma}_{\vec{k}}'^+, \quad \hat{c}_{\vec{k},\uparrow}^\dagger \hat{c}_{\vec{k},\uparrow} = \frac{1}{2} (\mathbb{1} + \hat{\sigma}_{\vec{k}}'^z), \quad \hat{c}_{\vec{k},\downarrow}^\dagger \hat{c}_{\vec{k},\downarrow} = \frac{1}{2} (\mathbb{1} - \hat{\sigma}_{\vec{k}}'^z). \quad (\text{C4})$$

These spin operators are denoted with a prime because we are still working in the un-dressed basis. Applying this mapping to our example term, we get

$$I_{\uparrow\uparrow} = \frac{V_{ee}}{4L} \sum_{\vec{k}, \vec{k}'} [1 - \cos(k_X - k'_X)] \hat{\sigma}_{\vec{k}}'^z \hat{\sigma}_{\vec{k}'}'^z + \frac{V_{ee}}{2} \sum_{\vec{k}} \hat{\sigma}_{\vec{k}}'^z. \quad (\text{C5})$$

Finally, we rewrite the model in the dressed basis. Since we have already mapped to a spin model, we simply apply the corresponding rotation to the spin operators,

$$\hat{\sigma}_{\vec{k}}'^x = \hat{\sigma}_{\vec{k}}^z, \quad \hat{\sigma}_{\vec{k}}'^y = -\hat{\sigma}_{\vec{k}}^y, \quad \hat{\sigma}_{\vec{k}}'^z = \hat{\sigma}_{\vec{k}}^x, \quad (\text{C6})$$

where the non-primed spin operators are the ones used in the main text. We end up with

$$I_{\uparrow\uparrow} = \frac{V_{ee}}{4L} \sum_{\vec{k}, \vec{k}'} [1 - \cos(k_X - k'_X)] \hat{\sigma}_{\vec{k}}^x \hat{\sigma}_{\vec{k}'}^x + \frac{V_{ee}}{2} \sum_{\vec{k}} \hat{\sigma}_{\vec{k}}^x. \quad (\text{C7})$$

### C.3. Full spin model

The same procedure is applied to the other interaction terms in the Fermi-Hubbard Hamiltonian. We convert the nearest-neighbour interaction of  $|\downarrow\downarrow\rangle$  atoms along the  $Y$  lattice direction,

$$V_{ee} \sum_{i,j} \hat{n}_{i,j,\downarrow} \hat{n}_{i,j+1,\downarrow} = \frac{V_{ee}}{4L} \sum_{\vec{k}, \vec{k}'} [1 - \cos(k_Y - k'_Y)] \hat{\sigma}_{\vec{k}}^x \hat{\sigma}_{\vec{k}'}^x - \frac{V_{ee}}{2} \sum_{\vec{k}} \hat{\sigma}_{\vec{k}}^x, \quad (\text{C8})$$

the nearest-neighbour  $|\uparrow\rangle - |\downarrow\rangle$  interaction along the  $X$  direction,

$$\begin{aligned} V_{\uparrow\downarrow} \sum_{i,j} (\hat{n}_{i,j,\uparrow} \hat{n}_{i+1,j,\downarrow} + \hat{n}_{i,j,\downarrow} \hat{n}_{i+1,j,\uparrow}) &= -\frac{V_{\uparrow\downarrow}}{2L} \sum_{\vec{k}, \vec{k}'} \cos(k_X - k'_X) (\hat{\sigma}_{\vec{k}}^y \hat{\sigma}_{\vec{k}'}^y + \hat{\sigma}_{\vec{k}}^z \hat{\sigma}_{\vec{k}'}^z) \\ &\quad - \frac{V_{\uparrow\downarrow}}{2L} \sum_{\vec{k}, \vec{k}'} \hat{\sigma}_{\vec{k}}^x \hat{\sigma}_{\vec{k}'}^x, \end{aligned} \quad (\text{C9})$$

the nearest-neighbour  $|\uparrow\rangle - |\downarrow\rangle$  interaction along the  $Y$  direction,

$$\begin{aligned} V_{\uparrow\downarrow} \sum_{i,j} (\hat{n}_{i,j,\uparrow} \hat{n}_{i,j+1,\downarrow} + \hat{n}_{i,j,\downarrow} \hat{n}_{i,j+1,\uparrow}) &= -\frac{V_{\uparrow\downarrow}}{2L} \sum_{\vec{k}, \vec{k}'} \cos(k_Y - k'_Y) (\hat{\sigma}_{\vec{k}}^y \hat{\sigma}_{\vec{k}'}^y + \hat{\sigma}_{\vec{k}}^z \hat{\sigma}_{\vec{k}'}^z) \\ &\quad - \frac{V_{\uparrow\downarrow}}{2L} \sum_{\vec{k}, \vec{k}'} \hat{\sigma}_{\vec{k}}^x \hat{\sigma}_{\vec{k}'}^x, \end{aligned} \quad (\text{C10})$$

and the on-site interaction,

$$U_{\uparrow\downarrow} \sum_{i,j} \hat{n}_{i,j,\uparrow} \hat{n}_{i,j,\downarrow} = -\frac{U_{\uparrow\downarrow}}{4L} \sum_{\vec{k},\vec{k}'} \vec{\sigma}_{\vec{k}} \cdot \vec{\sigma}_{\vec{k}'}.$$
(C11)

We also directly convert the single-particle terms in the Hamiltonian by writing them in momentum space, then using the mapping in Eq. (C4), then rotating via Eq. (C6). We have the tunneling,

$$\begin{aligned}
\hat{H}_J &= \sum_{i,j} \left( -J_0 \hat{c}_{i,j,\downarrow}^\dagger \hat{c}_{i+1,j,\downarrow} + J_1 \hat{c}_{i,j,\uparrow}^\dagger \hat{c}_{i+1,j,\uparrow} - J_0 \hat{c}_{i,j,\uparrow}^\dagger \hat{c}_{i,j+1,\uparrow} + J_1 \hat{c}_{i,j,\downarrow}^\dagger \hat{c}_{i,j+1,\downarrow} + h.c. \right) \\
&= \sum_{\vec{k}} \left[ -2J_0 \cos(k_X) \hat{n}_{\vec{k},\downarrow} + 2J_1 \cos(k_X) \hat{n}_{\vec{k},\uparrow} - 2J_0 \cos(k_Y) \hat{n}_{\vec{k},\uparrow} + 2J_1 \cos(k_Y) \hat{n}_{\vec{k},\downarrow} \right] \\
&= (J_1 + J_0) \sum_{\vec{k}} [\cos(k_X) - \cos(k_Y)] (\hat{n}_{\vec{k},\uparrow} - \hat{n}_{\vec{k},\downarrow}) + (J_1 - J_0) \sum_{\vec{k}} [\cos(k_X) + \cos(k_Y)] (\hat{n}_{\vec{k},\uparrow} + \hat{n}_{\vec{k},\downarrow}) \\
&= \sum_{\vec{k}} \epsilon_{\vec{k}} \hat{\sigma}_{\vec{k}}^x + \sum_{\vec{k}} \overline{E}_{\vec{k}} \mathbb{1},
\end{aligned} \tag{C12}$$

with the parameters  $\epsilon_{\vec{k}} = (J_1 + J_0)[\cos(k_X) - \cos(k_Y)]$  and  $\overline{E}_{\vec{k}} = (J_1 - J_0)[\cos(k_X) + \cos(k_Y)]$  defined as in the main text. We also have the drive,

$$\hat{H}_\Omega = \frac{\Omega}{2} \sum_{\vec{k}} \left( \hat{c}_{\vec{k},\uparrow}^\dagger \hat{c}_{\vec{k},\downarrow} + h.c. \right) = \frac{\Omega}{2} \sum_{\vec{k}} \hat{\sigma}_{\vec{k}}^z. \quad (\text{C13})$$

Putting all of these terms yields the spin model  $\hat{H}_S$  in the main text.

## D. COLLECTIVE SPIN MODEL DERIVATION

### D.1. Collective basis

Here we show how the spin model  $\hat{H}_S$  in the main text can be transformed into a collective one-axis twisting model. We start by splitting the spin model into pieces:

$$\begin{aligned}\hat{H}_S &= \hat{H}_0 + \hat{H}_{\text{int}}^{(\text{CS})} + \hat{H}_J, \\ \hat{H}_0 &= \hat{H}_{\text{int}}^{(\text{OS})} + \hat{H}_\Omega.\end{aligned}\quad (\text{D1})$$

The first piece  $\hat{H}_0$  consists of the Heisenberg term  $\sim U_{\uparrow\downarrow}$  from the on-site interactions and the drive  $\sim \Omega$ ,

$$\hat{H}_0 = -\frac{U_{\uparrow\downarrow}}{4L} \sum_{\vec{k}, \vec{k}'} \vec{\sigma}_{\vec{k}} \cdot \vec{\sigma}_{\vec{k}'} + \frac{\Omega}{2} \sum_{\vec{k}} \hat{\sigma}_{\vec{k}}^z. \quad (\text{D2})$$

The second piece consists of the cross-site interactions, which can be written as

$$\begin{aligned} \hat{H}_{\text{int}}^{(\text{CS})} = & \frac{1}{4L} \sum_{\vec{k}, \vec{k}'} [2V_{ee} - 4V_{\uparrow\downarrow} - V_{ee} (\cos(k_X - k'_X) + \cos(k_Y - k'_Y))] \hat{\sigma}_{\vec{k}}^x \hat{\sigma}_{\vec{k}'}^x \\ & - \frac{V_{\uparrow\downarrow}}{2L} \sum_{\vec{k}, \vec{k}'} [\cos(k_X - k'_X) + \cos(k_Y - k'_Y)] \left( \hat{\sigma}_{\vec{k}}^y \hat{\sigma}_{\vec{k}'}^y + \hat{\sigma}_{\vec{k}}^z \hat{\sigma}_{\vec{k}'}^z \right), \end{aligned} \quad (\text{D3})$$

and the third piece is the single-particle dephasing terms coming from the tunneling,

$$\hat{H}_J = (J_1 + J_0) \sum_{\vec{k}} [\cos(k_X) - \cos(k_Y)] \hat{\sigma}_{\vec{k}}^x. \quad (\text{D4})$$

The first piece  $\hat{H}_0$  contains the energetically-strongest terms, which we can write as a collective-spin Hamiltonian,

$$\hat{H}_0 = -\frac{U_{\uparrow\downarrow}}{L} \vec{S} \cdot \vec{S} + \Omega \hat{S}^z, \quad (\text{D5})$$

with  $\vec{S} = (\hat{S}^x, \hat{S}^y, \hat{S}^z)$ . As discussed in the main text, this Hamiltonian conserves total angular momentum  $S$  and creates an energy gap between the fully-symmetric Dicke manifold  $S = L/2$  and the next shell  $S = L/2 - 1$ . We can thus approximate the effect of the other two pieces  $\hat{H}_{\text{int}}^{(\text{CS})}$ ,  $\hat{H}_J$  on unitary evolution of fully-symmetric product states by projecting these pieces into the Dicke manifold via perturbation theory.

## D.2. Nearest-neighbour interaction terms

The nearest-neighbour interactions  $\hat{H}_{\text{int}}^{(\text{CS})}$  are easiest to start with because their dominant contribution is just their projection into the Dicke manifold directly. These interactions consist of two-body spin terms  $\hat{\sigma}_{\vec{k}}^\alpha \hat{\sigma}_{\vec{k}'}^\alpha$  (for  $\alpha \in \{x, y, z\}$ ), which can be turned into collective terms via

$$\hat{\sigma}_{\vec{k}}^\alpha \hat{\sigma}_{\vec{k}'}^\alpha \rightarrow (1 - \delta_{\vec{k}, \vec{k}'}) \frac{4}{L(L-1)} \hat{S}^\alpha \hat{S}^\alpha, \quad (\text{D6})$$

which amounts to ignoring the spin quasi-momentum indices unless the term involves a product of two equal spin operators in the same quasi-momentum mode, in which case the term equals the identity and is ignored. We divide by  $L(L-1)$  since the all-to-all  $\hat{S}^\alpha \hat{S}^\alpha$  consists of  $L(L-1)$  non-identity interaction terms compared to a single one, and multiply by 4 because of the factor of two difference between Pauli and spin operators. The momentum-dependent coefficients of the individual terms are averaged, causing any cosine terms to vanish, leaving

$$\hat{H}_{\text{int}}^{(\text{CS})} \rightarrow \frac{2}{L} (V_{ee} - 2V_{\uparrow\downarrow}) \hat{S}^x \hat{S}^x. \quad (\text{D7})$$

This collective term represents the dominant effect of the nearest neighbour interactions in the Dicke manifold. While there can also be higher order effects from the cross-site terms, we ignore them because the overall cross-site interaction coefficients are already small compared to the energy gaps set by  $\hat{H}_0$ .

## D.3. Tunneling terms

We now turn to the dephasing terms  $\hat{H}_J$  that come from the tunneling. We can likewise project these into the Dicke manifold by replacing  $\hat{\sigma}_{\vec{k}}^x$  with  $\frac{2}{L} \hat{S}^x$ . Because of the cosine prefactors, however, this projection will average to zero and the dephasing terms will have no zeroth-order effect. Their lowest-order contribution will instead come in as a second-order perturbation.

The standard second-order Schrieffer-Wolff correction to the Hamiltonian can be written as

$$\hat{H}_{J,\text{eff}} = -\frac{1}{2} [\mathcal{O} \hat{H}_J, \mathcal{L} \hat{H}_J], \quad (\text{D8})$$

where  $\mathcal{O} \hat{H}_J$  consists of all matrix elements of  $\hat{H}_J$  coupling *different* angular momentum  $S$ -shells, and

$$\mathcal{L} \hat{H}_J = \sum_{\alpha, \beta} \frac{1}{E_\alpha - E_\beta} |\alpha\rangle \langle \alpha| \mathcal{O} \hat{H}_J |\beta\rangle \langle \beta|, \quad (\text{D9})$$

where the sums  $\alpha, \beta$  run over all states in the Hilbert space and  $E_\alpha = \langle \alpha | \hat{H}_0 | \alpha \rangle$ ,  $E_\beta = \langle \beta | \hat{H}_0 | \beta \rangle$  are unperturbed state energies.

Since we are interested in dynamics that start with collective product states, to good approximation we can restrict our analysis to the Dicke manifold where the product states reside ( $S = L/2$ ) and the next-lowest angular momentum shell of spin-waves ( $S = L/2 - 1$ ). The Dicke states will be written in shorthand as  $|S = L/2, m\rangle = |m\rangle$  for  $m \in S, S-1, \dots, -S$ . The spin-wave states are labelled by an additional index  $k \in 1 \dots L-1$ , written in shorthand as  $|S = L/2 - 1, m, k\rangle = |mk\rangle$ . We write our perturbation theory terms using this shorthand:

$$\mathcal{O} \hat{H}_J = \sum_{m=-L/2}^{L/2} \sum_{m'=-L/2+1}^{L/2-1} \sum_{k=1}^{L-1} \left( |m\rangle \langle m'k| \langle m | \hat{H}_J | m'k \rangle + \text{h.c.} \right), \quad (\text{D10})$$

and

$$\mathcal{L} \hat{H}_J = \sum_{m=-L/2}^{L/2} \sum_{m'=-L/2+1}^{L/2-1} \sum_{k=1}^{L-1} \frac{1}{-U_{\uparrow\downarrow} + \Omega(m - m')} \left( |m\rangle \langle m'k| \langle m | \hat{H}_J | m'k \rangle - \text{h.c.} \right). \quad (\text{D11})$$

We evaluate the commutator of these two, yielding

$$\begin{aligned} \hat{H}_{J,\text{eff}} &= \frac{1}{2} \sum_{m=-L/2}^{L/2} \sum_{\tilde{m}=-L/2}^{L/2} \sum_{m'=-L/2+1}^{L/2-1} \sum_{k=1}^L \frac{1}{-U_{\uparrow\downarrow} + \Omega(m - m')} \left( |\tilde{m}\rangle \langle m| \langle \tilde{m}| \hat{H}_J |m'k\rangle \langle m'k| \hat{H}_J |m\rangle + h.c. \right) \\ &\quad - \frac{1}{2} \sum_{m=-L/2}^{L/2} \sum_{m'=-L/2+1}^{L/2-1} \sum_{k=1}^L \sum_{\tilde{m}'=-L/2}^{L/2} \sum_{\tilde{k}=1}^L \frac{1}{-U_{\uparrow\downarrow} + \Omega(m - m')} \left( |\tilde{m}'\tilde{k}\rangle \langle m'k| \langle \tilde{m}'\tilde{k}| \hat{H}_J |m\rangle \langle m| \hat{H}_J |m'k\rangle + h.c. \right). \end{aligned} \quad (\text{D12})$$

To evaluate these, we need the actual matrix elements of individual spin operators  $\hat{\sigma}_{k_X, k_Y}^x$  of which the perturbation consists. These are given by [42]

$$\langle m| \hat{\sigma}_n^x |m'k\rangle = \frac{e^{2\pi i k n / L}}{2} \left( -\sqrt{\frac{(\frac{L}{2} + m)(\frac{L}{2} + m - 1)}{L^2(L-1)}} \delta_{m,m'+1} + \sqrt{\frac{(\frac{L}{2} - m)(\frac{L}{2} - m - 1)}{L^2(L-1)}} \delta_{m,m'-1} \right), \quad (\text{D13})$$

where  $n \in 1 \dots L$  labels all of the spins using whatever indexing is convenient. For example, since we are working in 2D we write  $n = L_X(\frac{L_X}{2\pi}k_Y - 1) + \frac{L_X}{2\pi}k_X$  for conventional quasimomenta  $k_X \in \frac{2\pi}{L_X}\{1, 2, \dots, L_X\}$  and  $k_Y \in \frac{2\pi}{L_Y}\{1, 2, \dots, L_Y\}$ . Inserting these matrix elements into the sums above leads to

$$\begin{aligned} \hat{H}_{J,\text{eff}} &= -\frac{2(J_0 + J_1)^2 U_{\uparrow\downarrow}}{(L-1)(U_{\uparrow\downarrow}^2 - \Omega^2)} \sum_{m=-L/2}^{L/2} m^2 |m\rangle \langle m| \\ &\quad + \frac{(J_0 + J_1)^2 U_{\uparrow\downarrow}}{(L-1)(U_{\uparrow\downarrow}^2 - \Omega^2)} \sum_{m=-L/2}^{L/2-2} \sqrt{\left(\frac{L}{2} + m + 2\right) \left(\frac{L}{2} + m + 1\right) \left(\frac{L}{2} - m\right) \left(\frac{L}{2} - m - 1\right)} (|m+2\rangle \langle m| + h.c.) \\ &\quad - \frac{2(J_0 + J_1)^2 \Omega}{U_{\uparrow\downarrow}^2 - \Omega^2} \sum_{m=-L/2}^{L/2} m |m\rangle \langle m|. \end{aligned} \quad (\text{D14})$$

These sums can all be identified with simple collective-spin terms. The first two lines correspond to a twisting term  $\hat{S}^x \hat{S}^x$ , while the last line is a single particle term. We thus get

$$\hat{H}_{J,\text{eff}} = \frac{1}{L-1} \frac{4(J_0 + J_1)^2 U_{\uparrow\downarrow}}{U_{\uparrow\downarrow}^2 - \Omega^2} \hat{S}^x \hat{S}^x - \frac{2(J_0 + J_1)^2 \Omega}{U_{\uparrow\downarrow}^2 - \Omega^2} \hat{S}^z. \quad (\text{D15})$$

This is the second-order perturbative contribution of the tunneling to the model's time-evolution. The first piece is a twisting term, while the second piece is just a correction to the diagonal single-particle drive frequency. Note that the single-particle correction is negligible compared to the bare magnitude of the drive  $\Omega$ , and we will neglect it, keeping only the twisting term.

#### D.4. Full collective model

We have now evaluated the zeroth-order contributions from the cross-site interactions  $\hat{H}_{\text{int}}^{\text{CS}}$  and the perturbative, second-order contributions from tunneling  $\hat{H}_{J,\text{eff}}$ . Adding these to the unperturbed  $\hat{H}_0$  yields the following collective model:

$$\begin{aligned} \hat{H}_{\text{OAT}} &= -\frac{U_{\uparrow\downarrow}}{L} \vec{S} \cdot \vec{S} - 2\chi \hat{S}^x \hat{S}^x + \Omega \hat{S}^z, \\ \chi &= \frac{1}{L-1} \frac{2(J_0 + J_1)^2 U_{\uparrow\downarrow}}{\Omega^2 - U_{\uparrow\downarrow}^2} - \frac{1}{L} (V_{ee} - 2V_{\uparrow\downarrow}), \end{aligned} \quad (\text{D16})$$

with  $\chi$  same as in the main text. This is a "twist-and-turn" model containing a one-axis twisting term, and a drive that it does not commute with. However, since the drive term  $\sim \Omega \hat{S}^z$  is much stronger than the squeezing rate  $\chi$ , we can make a rotating-wave approximation,

$$-2\chi \hat{S}^x \hat{S}^x \approx -2\chi \left[ \frac{1}{2} (\hat{S}^+ \hat{S}^- + h.c.) \right] = -\chi \vec{S} \cdot \vec{S} + \chi \hat{S}^z \hat{S}^z. \quad (\text{D17})$$

The  $-\chi \vec{S} \cdot \vec{S}$  portion of this is small compared with the bare  $\frac{U_{\uparrow\downarrow}}{L} \vec{S} \cdot \vec{S}$  term and can be neglected. Note that any  $\vec{S} \cdot \vec{S}$  term amounts to a constant energy shift when within the Dicke manifold anyways, and we only keep it in the Hamiltonian to emphasize the gap protection preventing leakage into other manifolds. This leaves us with

$$\hat{H}_{\text{OAT}} \approx -\frac{U_{\uparrow\downarrow}}{L} \vec{S} \cdot \vec{S} + \chi \hat{S}^z \hat{S}^z + \Omega \hat{S}^z, \quad (\text{D18})$$

which is the one-axis twisting model  $\hat{H}_{\text{OAT}}$  in the main text.

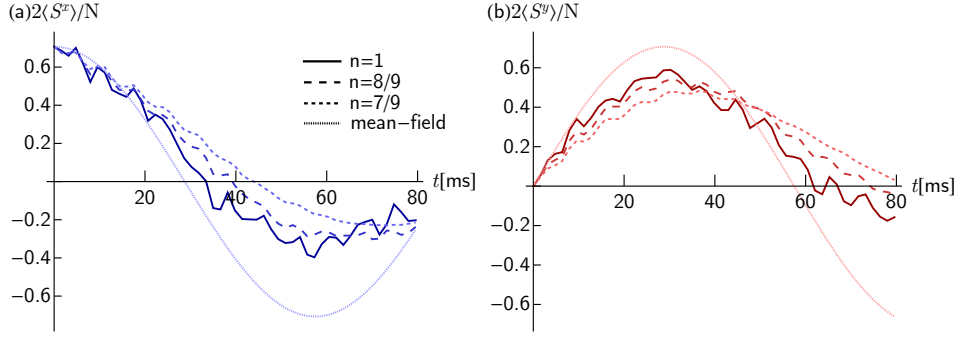


FIG. S4. Density phase shift precession measured by (a)  $\langle \hat{S}^x \rangle$  and (b)  $\langle \hat{S}^y \rangle$  for  $L = 3 \times 3$  systems with holes in the initial loadout. We assume all lattice sites have a  $|g\rangle$  atom, but that some are missing an excited-band atom acting as the spin-1/2. The  $n = 1$  has ideal filling, while  $n = 8/9$  has no excited atom at lattice site  $(i, j) = (3, 3)$  (using periodic boundaries), and  $n = 7/9$  no excited atoms at  $(3, 3)$  and  $(1, 2)$ . The mean-field lines show the ideal oscillation envelopes with no contrast decay (the expected behaviour in the  $L = N \rightarrow \infty$  limit).

### E. IMPERFECT FILLING FRACTION

The energetic gap of a band insulator has allowed for fidelity of over 99% in the central ten-by-ten core of a two-dimensional optical lattice [43]. The remaining holes will introduce errors in our protocol, as they facilitate mode-changing collisions that invalidate the spin model approximation. However, with a sufficiently low defect density, we still expect to observe a collective-spin signal from the p-wave interactions. Figure S4 shows the density phase precession of the collective spin using the protocol in the main text, for initial conditions that have one or more holes in place of the excited atoms (still assuming a filled ground band). For a sufficiently low hole fraction, the amplitude of oscillation is somewhat reduced, but one can still infer the oscillation period set by  $\chi$ .